International Journal of MATERIALS RESEARCH Zeitschrift für METALLKUNDE Original Contributions

A. Das: An artificial intelligence paradigm in heuristic search of tensile behaviour of titanium alloys

Arpan Das

Mechanical Metallurgy Division, Materials Group, Bhabha Atomic Research Centre (Department of Atomic Energy), Trombay, Mumbai, Maharashtra, India

An artificial intelligence paradigm in heuristic search of tensile behaviour of titanium alloys

Fracture properties of materials are strongly influenced by initial microstructure/texture, loading conditions, environment, notch geometry and phase transformations. The notch geometry effect on fracture properties of materials is very sensitive to the geometry of structure, scale effects and loading mode. A critical literature review is performed to understand several consensuses about the complexity of notch geometry in the deformation and fracture responses of materials. It is still not clear in these circumstances which variable is the most important to determine the mechanical properties of materials. This article deals with the quantitative methods for designing specimen geometry for different applications. However, microstructure alone is not a sufficient parameter for designing new alloys. In this work, the effect of notch geometry and temperature on the tensile properties of titanium alloys has been determined through a Bayesian computational framework under an artificial intelligence paradigm. The dataset considered for computation is essentially obtained from the elegant experimental research of Jenkins and Willard. Their analysis was performed on a physical basis and gives very clear indications to designers about the influence of temperature and specimen geometry on the mechanical properties of the alloys. The engineering significance of both the results is compared comprehensively. The present models have been applied to corroborate that the calculations are reasonable in the context of established solid mechanics and metallurgical theories. It has also been possible to gauge the isolated influence of particular variables such as elastic stress concentration factor, which exactly cannot in practice be varied independently. This highlights the ability of the technique

to examine the new phenomena in cases where information cannot be accessed experimentally. This model will be instrumental for mechanical engineers to design critical industrial components.

Keywords: Fracture; Notch geometry; Titanium alloys; Neural computation; Stress triaxiality.

1. Introduction

Research on fracture mechanics deals with the story of crack propagation/branching and the estimation of unstable fracture of crack-containing structures; hence it is often employed in industry for assessing the safety of those components [1, 2]. Ascertaining a common criterion which can predict the mechanical failure of these structural parts is one of the crucial concerns for engineers [3]. The gate of fracture mechanics research was firstly opened by the pioneering work of Griffith [4]. Fracture behaviour of any component in a structure is often influenced by a combination of geometry/design, microstructure/texture, service temperature/environment and different loading conditions. The geometry and crack configurations influence the fracture response of a material tremendously.

Mechanical behaviour of a structural component under any external load may be strongly affected by the presence of different geometrical discontinuities such as fillets, grooves, threads, cracks etc. These local geometrical perturbations lead to local increase in stress/strain fields around them. The role of these stress raisers on deformation/flow responses of a material is of prime importance in mechanical design. In the 17th century, when Galileo, the inventor of the concept of stress, foremost, employed combined mathematical and experimental methodologies to investigate the fracture behaviour of solids [2, 5-7]; there he found that fracture occurs along the plane with the maximum active normal stresses. Classical research, commonly performed by structural engineers, can be evidently found in the articles of Norton [8], Roark and Young [9], Budynas and Nisbett [10], Inglis [11], where emphasis was mostly given to the complex elastic stress concentration theories and related problems. The importance of notched structural members under monotonic deformation has led to a vast body of research in the rich works of Coker et al. [12], Howland [13], Strandberg [14] and Zappalorto et al. [15]; mainly focusing on evaluating the stress intensity factors around the geometrical perturbations. The lack of a universal understanding of notch geometry effect on the mechanical properties of materials may originate from the lack of universal fracture criterion applicable for all kinds of materials ranging from ductile crystalline/polycrystalline metals to brittle ceramics, as explained by Qu et al. [16]. Zhang and Eckert [5, 17] proposed a widely accepted criterion, namely the ellipse criterion, which has proved to be unified fracture theory unifying the classical four criteria i.e., the maximum normal stress, Tresca, von-Mises and Mohre Coulomb. Recently, the ellipse criterion was further extended into a universal fracture criterion, as proposed by Qu and Zhang [18] in their pioneering research.

The notch is a very important geometry with prevalent applications in engineering and structural components. The one source of stress concentration in industrial components, it plays a crucial role in safety design of engineering materials. Different conditions of notch effect on the strength of materials (see Fig. 10 [16]) by the ellipse criterion have already been demonstrated by Qu et al. [16] elsewhere. The primary motivation is that adopting the notched specimen produces localised stress at the root of notches, resulting in well-controlled crack extension from the source of tip (see Fig. 10 [16]). When the crack location/configuration in a component can be controlled (through design), it is highly possible to avoid unexpected fracture. Lorenzino and Navarro [19] found that for the same specimen geometry and loading type, the influence of stress concentration is directly dependent on the notch geometry and grain size of the material. They investigated how the probability of failure rapidly increases with increasing notch root radius (RR). In order to design the optimum specimen geometry, understanding the crack extension behaviour of a notched tensile specimen is essential. Nozawa and Tanigawa [20] noticed that there is no significant specimen size effect for certain test conditions for composites. Recently, Kumar et al. [21] experimentally optimised the thickness of miniature tensile specimens for the evaluation of mechanical properties of low alloy steels under ambient temperature and constant strain rate. The current study, therefore, primarily emphasises clarifying the effect of notch geometries to the tensile properties of materials; considering the notch sensitivity of a titanium alloy at different testing temperatures usually employed in industries. There are publications, where results make clear that the actual physical size of a notch does not seem to be as important as the relative size of the notch with respect to the characteristic of micro-

structural dimensions [19, 22]. Many variables have been found to influence the fracture process of materials; some of them are related to the specimen geometry, such as the size effect [21, 23, 24], while some others are related to the stress-state [21, 25–32] and the microstructural properties of materials, such as work hardening [33–48], anisotropy/texture [49–58] and the morphology/characteristics of microstructures [33-47, 49-58]. Geometry necessarily controls the stress-state and strain-state of the specimens during loading [21, 32]. Varying the geometries is, therefore, largely used to investigate fracture mechanisms of materials. Size effects in fracture mechanics have received much attention in recent years [21, 32, 59, 60]. Size effects observed in cracked and/or notched specimens are closely related to the size of plastic zone with respect to the specimen dimensions and material heterogeneities. Exhaustive figures and tables have been published on the 'stress-concentration factor' by Pilkey [61] and Young et al. [62] which account for a wide variety of possible specimen configurations. Chang et al. [63] introduced a progressive damage evolution/assessment model for notched laminates subjected to monotonic loading.

Titanium alloys offer attractive mechanical/fracture properties such as high strength to weight ratio, good creep, fatigue resistance at high temperatures, excellent corrosion resistance, high formability and good biocompatibility; hence are widely being utilised in different applications. These alloys are one of the most preferred and accepted materials for aerospace, biomedical, chemical and petrochemical industries. These alloys are high performance materials subjected to severe and complex service conditions. Among all these, Ti-8Al-1Mo-1V is a near α titanium alloy which is characterised by low density, high Young's modulus, excellent damping capacity, good microstructural stability and extraordinary welding and moulding performances [64]. Therefore, Ti-8Al-1Mo-1V alloy is an important material in various industries, such as gas turbine, power plant and aerospace applications [65, 66]. Understanding the critical behaviour of these alloys is complicated through variations in operating temperature and notch geometries, which have been shown to change the relative activation of deformation and fracture properties. Thus, it is evident that the deformation and fracture behaviour of titanium alloys are strongly affected by service temperature and notch geometry where the microstructures and textures are not trivial. This critical point may be dependent on the detailed situation for plastic deformation ahead of a notch, which originally depends on the material's nature and common behaviour.

Tensile experiments are commonly performed using notched cylindrical solid specimens to evaluate the effect of stress triaxiality and uniaxial tensile properties to the notch strength ratio (NSR). In designing the monotonically loaded notched components out of the standard structural materials, it is a very common engineering practice to ignore the stress concentrations entirely, because they will be blunted by plastic flow before the component fails. In their elegant research work, Jenkins and Willard [67] conducted a careful series of experiments to see the effect of temperature and notch geometry on the tensile behaviour of a Ti-8Al-1Mo-1V alloy. Notwithstanding the large volume of experimental evidence on these, there exists an obstacles to understanding the effect of notch geometry and testing temperature on the deformation and fracture proper-

ties of this alloy under tensile deformation completely. There is no adequate theory in the published domain to deal with this task, which is the correlation of tensile properties as a function of notch geometry and testing temperature. A difficult problem like this, where the general concepts might be understood but which are not as yet amenable to the fundamental treatment, are common in solid mechanics. To form a complete story, it is necessary in such circumstances to resolve the problem through learned empiricism. The combination of physical and empirical models with understanding of solid mechanics and related theory of metallurgy can then be employed to attempt the design of structural components. This is an important scientific issue in materials science and solid mechanics fields because it involves detail of both the material microstructure and the mechanical stress/deformation fields due to notch geometry variations which develop for given microstructural conditions.

Many authors have already discussed the mechanisms of fracture in components containing smooth stress concentrations, and several criteria have already been widely proposed by different researchers for predicting failure. When a notched bar is loaded in plane strain bending, plastic zones form at the notch root tip and spread into ligaments with progression of loading severity. These zones have the form of logarithmic spirals [68, 69] predicted by the classical slip line field theory of Hill [70]. The method used in this research is neural computation for empirical analysis. Neural computation is capable of replicating a huge variety of non-linear relationships. Neural networks consist of simple synchronous processing elements, which are inspired by biological nerve systems. Data are presented/incorporated to the network in the form of input and output parameters, and the optimum non-linear relationship is found by minimizing the differences between the measured value and the calculated one. As in common regression analysis, the results then consist of a series of co-efficient and a specification of the type of function used which, in combination with weights, relates the inputs to the output. To prevent over fitting, MacKay [71-74] has developed the elegant Bayesian framework to control the complexity of a neural network. This framework also supplies the quantified error bars on the network predictions and renders it possible to identify automatically which of the many relevant input variables are in fact important factors in the regression analysis. This specific technique has been comprehensively reviewed in Refs. [75–78] and discussed thoroughly in different applications [79–85], hence will not be discussed further except in the context of the current analysis.

The problem of evaluating tensile properties of materials clearly involves many variables, their mutual (and/or unknown) interactions and considerable complexity. The analysis performed on an experimental basis in the article of Jenkins and Willard [67] gives very clear indications to designers on the influences of temperature and specimen geometry to the tensile behaviour of Ti-8Al-1Mo-1V alloy. The purpose of the present research is not only to identify the parameters which control the tensile properties of Ti-8Al-1Mo-1V alloy but also to correlate the complex relationship between the tensile properties of materials with their influencing parameters. In this work, the influence of each individual variable on tensile properties of Ti-8Al-1Mo-1V alloy will be investigated with different notch geometries

and test temperatures. There are limited studies available in the public sphere to exactly know the effective and relative contributions of these factors to the mechanical properties of these alloys. In the present context, the optimisation of different tensile properties (i.e., strength and ductility) needs access to a quantitative relationship between the notch angle (NA), root radius (RR), notch depth (ND), elastic stress concentration factor (ESCF) and temperature (T) of tensile tests. Several neural network models have been created to correlate different tensile properties individually with respective influencing parameters and employed extensively for applications within the Bayesian framework [71-85]. The present work as undertaken, therefore, aiming to clarify the "notch geometry - temperature - tensile property" relationship in a Ti-8Al-1Mo-1V alloy, and to identify the variables controlling the tensile properties. These approaches, combined with metallurgical and solid mechanics theories have been used here to model the deformation and fracture behaviour of titanium alloys. Both the methods (experiments and neural computation) are also comprehensively compared.

2. Data and variables

The introduction of a notch in an engineering component/ test-specimen develops stress concentration, which dramatically reduces the ductility of materials [1-6]. Comparing the circumstances of tensile deformation, it is apparent that the notch has a noteworthy impact on the stress-state/ strain-state induced in the specimens during experiments [67]. In smooth tensile specimens, the stress and strain are uniaxial in nature (under tension), whereas in the notched specimens they are complex and triaxial in nature (around the notch tip). This has a significant influence on the conditions of the entire experiment. In a standard tensile test, the specimens are generally smooth without any notches. Therefore, the induced stress can be straightforwardly calculated by dividing force by the cross-sectional area which is constant throughout the specimen gauge length. In notched specimens, the cross-sectional area varies with length dimensions depending on the shape of notch and it varies with its depth. Consequently, the deformation locally increases by decreasing the total elongation of the specimen and inducing an additional circumferential stress.

The material history, specimen geometry and test procedures are already explained by Jenkins and Willard in their elegant article [67]. Experimental data were digitised and collected from the published literature on the effect of testing temperature and notch geometry on the tensile properties of titanium alloys [67]. Uniaxial tensile tests (at constant strain rate of 0.01 min⁻¹) were conducted by Jenkins and Willard [67] on many unnotched and axisymmetric notched specimens having different sizes and geometries with different testing temperatures. Geometry effects were experimentally researched using specimens with various notch geometries, thus inducing different stress triaxiality levels. The ranges of various parameters in the dataset are listed in Table 1. Figures 4-10 from Ref. [67] were digitized to get the mechanical properties data (YS-Yield Strength, UTS-Ultimate Tensile Strength, TFS-True Fracture Stress, RA-Reduction in Area) as a function of notch angle (NA), root radius (RR), notch depth (ND), temperature of test (T) and elastic stress concentration factor (ESCF). The entire statistics of tensile properties data as a function of notch geometries and test temperature are also presented in Table 1. They are arranged systematically in a spread sheet for four different models (YS-Model, UTS-Model, TFS-Model and RA-Model) as a function of influencing parameters: NA, RR, ND, T, ESCF. The stress concentration, observed around the notch tip, is quantified by the stress concentration factor. This quantity is normally calculated there [86] analytically and/or numerically and is an important design parameter. These variables always determine the microstructure and mechanical properties of materials, the key components of any design process.

The aim of the current research is to predict YS, UTS, RA and TFS as functions of different notch geometries and test-

ing temperatures of a Ti-8Al-1Mo-1V alloy. A representative microstructure of the material shown in literature [67] indicates the presence of equiaxed alpha with stringers of Widmanstätten structure composed of alpha and beta (small) phases. Table 1 shows the range, mean, and standard deviation of each variable, including the outputs for all the four different neural network models created. The purpose here is simply to list the variables and provide an idea of the range covered in neural computations. However, it is emphasized that, unlike in linear regression analysis, the information given in Table 1 cannot be utilized to define the range of applicability of the present neural network models. This is because the inputs are in general expected to interact with each other. It is the Bayesian framework

Table 1. Statistics of the database used [67] for neural network analysis.

			YS-Model			
Inputs	Units	Maximum	Minimum	Mean	SD	Example
NA	0	180	0	67.28	36.25	60
T	$^{\circ}\mathrm{C}$	648.89	23.89	416.28	207.14	426.67
RR	mm	25.40	0.08	2.71	5.83	2.54
ND	%	85	0	45.73	21.49	10
ESCF	_	6.7	1	2.58	1.54	1.4
Output	Units	Maximum	Minimum	Mean	SD	Example
YS	MPa	1 557.92	235.21	784.91	322.95	
		•	UTS-Model			•
Inputs	Units	Maximum	Minimum	Mean	SD	Example
NA	0	180	0	67.28	36.25	60
T	°C	648.89	23.89	416.28	207.14	426.67
RR	mm	25.4	0.08	2.71	5.83	2.54
ND	%	85	0	45.73	21.49	10
ESCF	_	6.7	1	2.58	1.54	1.4
Output	Units	Maximum	Minimum	Mean	SD	Example
UTS	MPa	1 677.16	322.43	856.34	307.45	
•		•	RA-Model	•	•	•
Inputs	Units	Maximum	Minimum	Mean	SD	Example
NA	Ō	180	0	67.28	36.25	60
T	$^{\circ}\mathrm{C}$	648.89	23.89	416.28	207.14	426.67
RR	mm	25.4	0.08	2.71	5.83	2.54
ND	%	85	0	45.73	21.49	10
ESCF	_	6.7	1	2.58	1.54	1.4
Output	Units	Maximum	Minimum	Mean	SD	Example
RA	%	87.56	4.08	32.99	19.16	
		•	TFS-Model		•	•
Inputs	Units	Maximum	Minimum	Mean	SD	Example
T	°C	648.89	23.89	430.79	199.53	426.67
RR	mm	12.7	0.08	2.25	3.27	2.54
ND	%	85	0	46.25	24.59	10
ESCF	_	6.7	1	2.56	1.66	1.4
Output	Units	Maximum	Minimum	Mean	SD	Example
	MPa	1912.54	232.06	1 087.88	368.74	

[71–85] of the current neural network analysis that permits the deduction of error bars which define the range of useful applicability of the trained network, as described in the next section. The visual impression of the spread of data (Table 1) in 3D graphs is shown in Figs. 1–4 and latter in 2D graphs in Fig. 7 (a, c, e, g, i), Fig. 10 (a, c, e, g, i), Fig. 13 (a, c, e, g) and Fig. 16 (a, c, e, g, i) correspondingly. It is very clear from all these graphs that input variables are interactive with each other (unknown/complex interactions) during tensile deformation. It can be concluded from these figures that the effects on YS, TFS, RA, UTS of notch geometry and testing temperature have been systematically investigated by Jenkins and Willard [67] in their pioneering research. In the present study, both experimental and computationally calculated results are compared and discussed thoroughly.

3. Artificial intelligence

A common technique for solving complex problems is neural computation under a Bayesian framework of artificial intelligence. This has been systematically reviewed/applied in different metallurgical problems [71–85], designing of different alloys [71–85] and applied extensively in this current research. For this motivation, only specific points of importance are introduced in the current context.

Most of the research community is familiar with the common regression analysis where the data are best fitted to a particular correlation which is typically linear in nature. Neural networks now encompass a general and frequently used method of non-linear regression analysis in which a mathematical relationship is customary between each of the independent input variables, x_j and one or several dependent output variables, y. In linear regression analysis, the sum of all products, x_j is multiplied by a weight, w_j and a constant θ , giving an estimate of:

$$y = \Sigma_i w_i x_i + \theta \tag{1}$$

Neural networks are in broad-spectrum non-linear and this culminates in taking a hyperbolic tangent (tanh) function of the right hand side of this equation (Eq. (1)), and then applying a linear transfer into y. In fact, many hyperbolic tangent functions and related weights can be added to formulate the function to be as complex as is required. The relationship is simply fostered by presenting a neural network with a database (experiments) consisting of a set of inputs for which the value is known. The network then understands/learns the relationship (through repetitive representation) between the inputs and the corresponding values for the output in a route, which is usually recognized as training the network. Once the network is trained completely, output estimation for any given inputs is very rapid.

Linear functions of the inputs x_j are operated by the hyperbolic tangent transfer function (Eq. (2)):

$$h_i = \tan h(\Sigma_j w_{ij}^{(1)} + \theta_i^{(1)})$$
 (2)

so that each input adds/adjoins a contribution to the every hidden unit. The bias is denominated as θ_i and is analogous to the constant that appears in the linear regression analysis. The strength of the transfer function is in each case re-

solved/decided by the weight w_{ij} . The transfer to output y is then linear (Eq. (3)):

$$y = \Sigma_{i} w_{ii}^{(2)} + \theta^{(2)} \tag{3}$$

The specification of neural network structure explained, together with the set of weights is an absolute description of the formula correlating inputs to the output.

For instance, it is well established that the effect of notch root radius (*RR*) on the mechanical properties of titanium alloys is quite different at large values than that at smaller values, reported in literature [67, 87]. Regular and commonly applied regression analysis cannot cope with such variations in the form of relationships. A possible difficulty with the use of powerful regression analysis is the chance of overfitting the experimental data. For example, one can create a potential neural network model for a completely random set of experimental data. To circumvent such complexity, this experimental data can be sub-divided into two sub-sets, a training dataset and a testing dataset. The model is created using only the training experimental data set. The test data are then used to check that the model behaves itself when presented with formerly unseen data.

Neural networks in numerous ways mimic human experiences and are competent in learning or being trained to address the correct science rather than nonsensical trends. Unlike human experiences, these models can be transferred readily between generations and steadily developed to make design tools of lasting value. These models also impose a discipline on the digital retention of precious experimental data, which may otherwise be lost with the passage of time. The technique is extremely powerful and useful in any field of research. Detailed description of this can be found in literature [75-78] but it is important to note that the precision of model on unseen experimental data has been tested extensively against large quantities of information. All the input and output variables were normalised within the range of ± 0.5 . The normalisation is not necessary for the analysis but it facilitates the subsequent comparison of the significance of each of the variables. The normalisation is straightforward for all the quantitative variables. The entire data set was subjected to neural network analysis as an accepted technique of deciphering the independent roles of notch geometries and testing temperature in stimulating deformation and fracture behaviour of titanium alloys. Here, neural network technique under the Bayesian framework has been employed to solve this problem. In the current formulation, the complete network architecture is described in Table 2. The Bayesian framework has been expansively discussed in literature [71-85] and reviewed in articles [75-79]. Suffice it to explain that it is the crucial tool for non-linear regression analysis, and its predictions are coupled not only with an average measure of scatterdata but, more importantly in the current circumstance, also a modelling uncertainty which describes the ambiguity with which different empirical models can express the same set of experimental data. In the current models, it has been possible to show the isolated influence of individual input variables to the respective outputs (YS, UTS, TFS, RA). The Bayesian neural network has an excellent advantage to calculate the significance of each input variable which has been clearly demonstrated by MacKay [71–74] in his pioneering research.

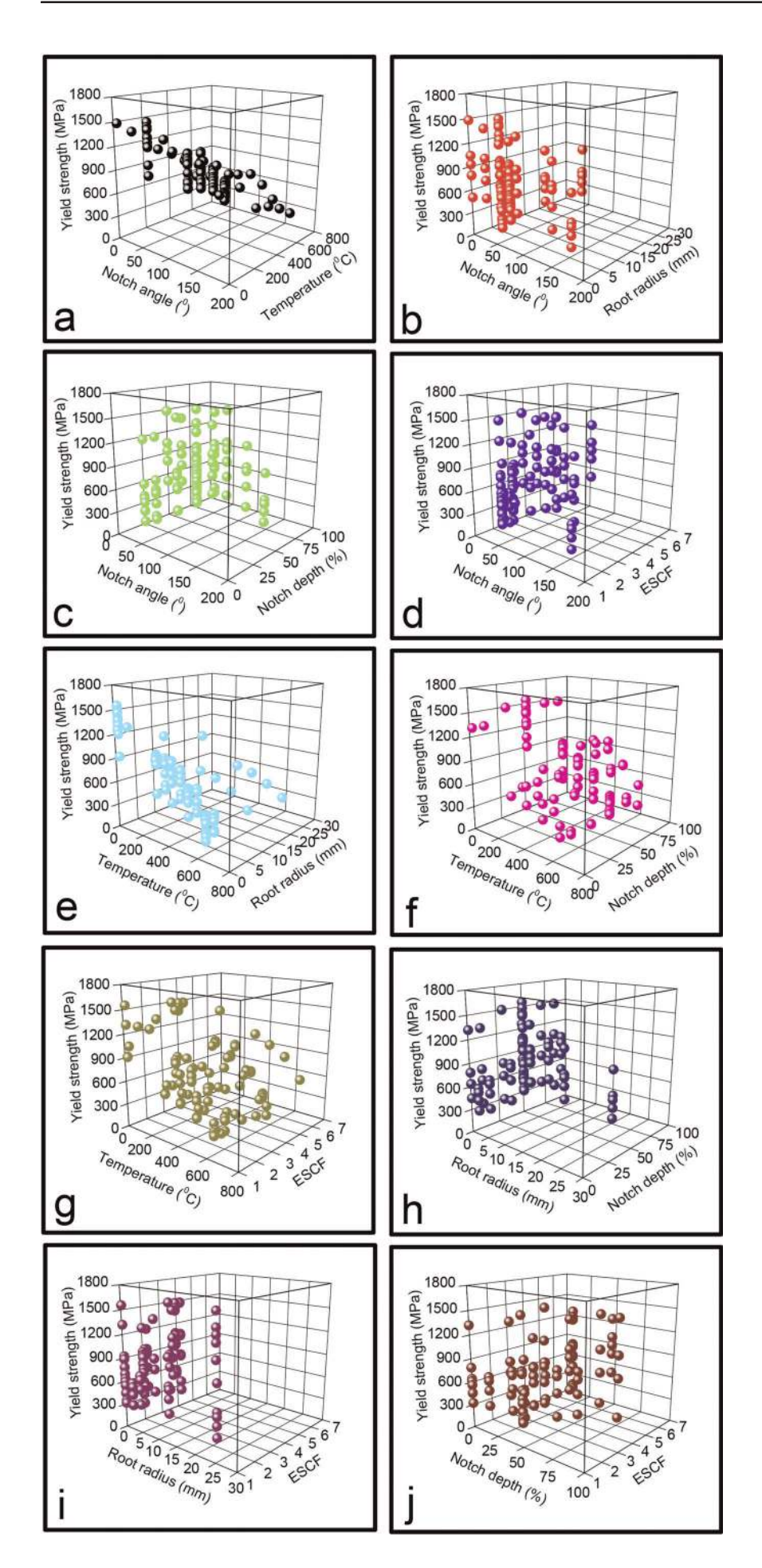


Fig. 1. Possible interactions of influencing variables with YS during tensile deformation of Ti-8Al-1Mo-1V alloy in 3D plots made from the experimental data reported by Jenkins and Willard [67].

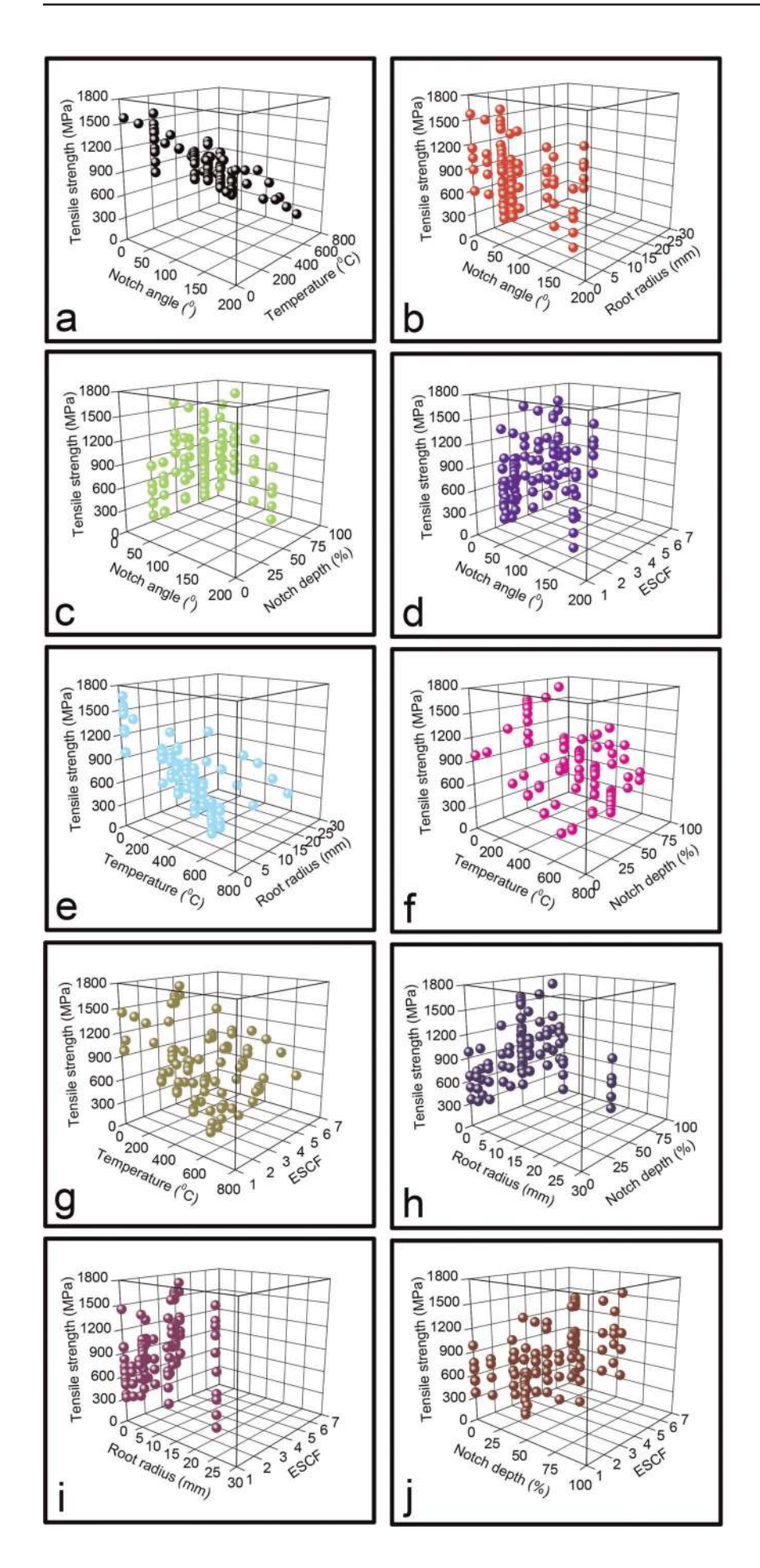


Fig. 2. Possible interactions of influencing variables with *UTS* during tensile deformation of Ti-8Al-1Mo-1V alloy in 3D plots made from the experimental data reported by Jenkins and Willard [67].

4. Results and discussion

4.1. Yield strength model

Some 100 different YS models were trained (Fig. 5a) with a training dataset which consisted of a random selection of 52 experiments. The remaining 51 dataset configures the test dataset (Fig. 5b), which has been employed to observe how the model generalises on the unseen data. Each model contained the five inputs listed in Table 2 but with different numbers of hidden units or the random seeds/neurons employed to instigate the values of weights. Figure 5a-f shows the entire YS-Model related results. As anticipated, the perceived level of noise, σ_{v} in the normalized YS data decreases as the model becomes more complex, i. e., the number of hidden units increases (Fig. 5d). This is not the case for test error (T_e) , which goes through a minimum at thirteen hidden units (Fig. 5e), or for the log predictive error (LPE), which reaches a maximum at six hidden units (Fig. 5c).

The number of hidden units used determines the complexity of neural computation and more reliable predictions occur with increased number of hidden units. Error bars throughout the current analysis represent a combination of perceived level of noise, $\sigma_{\rm v}$ in the output and fitting uncertainty evaluated from the Bayesian computations. It is strictly apparent that there are few outliers in the plot of the calculated versus measured YS for test dataset (Fig. 5b). Each of these outliers has been investigated and found to represent unique data not represented in the training dataset (Fig. 5a). When applying noisy data, common in many experimental situations, some wild predictions would be anticipated.

It is greatly possible that a committee of models can make a more genuine prediction rather than an individual model [71–74]. The best models are ranked using the values of LPE (Fig. 5c). Committees are then constructed by combining the predictions of the best L models, where L=1, 2, 3...; size of the committee is, therefore, given by the value of L. A plot of test error (T_e) of the committee versus its size offers a minimum which defines the optimum size of committee, as shown in Fig. 5f. Test error (T_e) associated with the best single model is convincingly greater than that of any of the committees (Fig. 5f). A committee

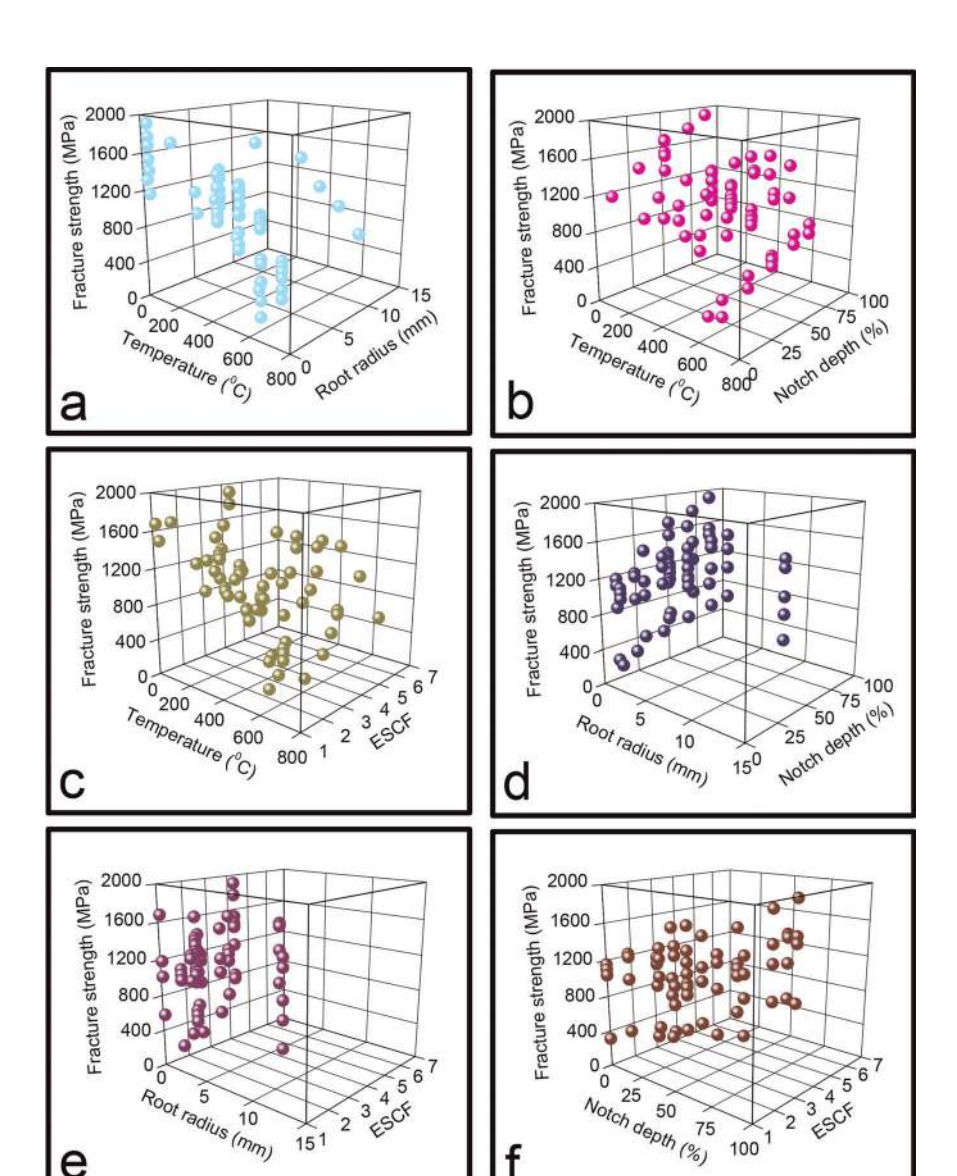


Fig. 3. Possible interactions of influencing variables with *TFS* during tensile deformation of Ti-8Al-1Mo-1V alloy in 3D plots made from the experimental data reported by Jenkins and Willard [67].

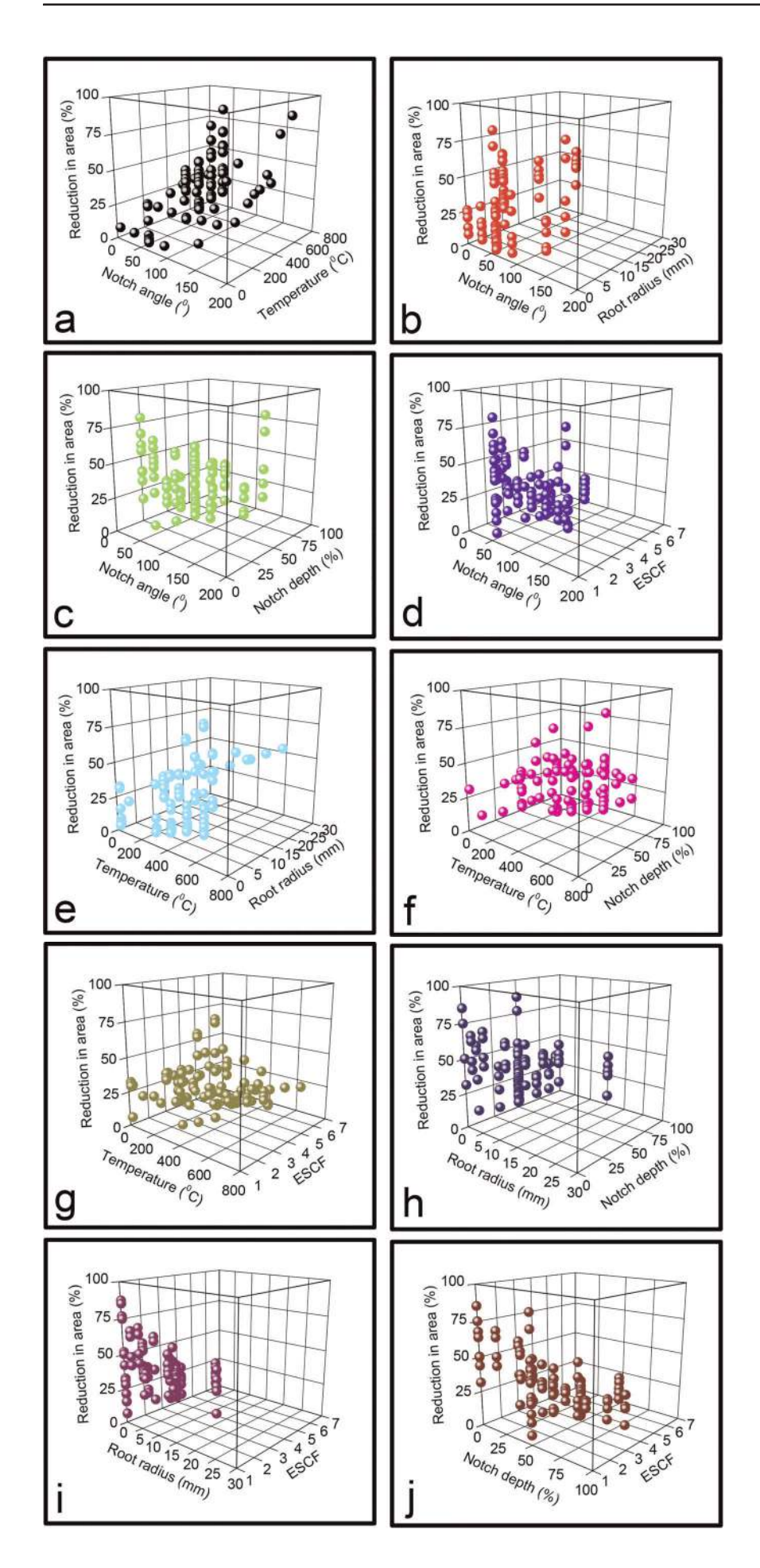


Fig. 4. Possible interactions of influencing variables with *RA* during tensile deformation of Ti-8Al-1Mo-1V alloy in 3D plots made from the experimental data reported by Jenkins and Willard [67].

with 93 models was found to have an optimum membership with the smallest test error $(T_{\rm e})$ (see Fig. 5f). The committee was, therefore, retrained on the entire dataset without changing the complexity of any of its member-models' parameters. The final comparison between the calculated and measured values of YS for the committee of 93 models is shown in Fig. 6a. Details of the 93 members of the optimum committee are given in Table 2.

The predictions applying the optimum committee of models are exhibited in Fig. 6a. The application of YS-Model is manifested in Figs. 6b and c which imply that the model behaves robust for the unseen experimental data. Figure 6d compares the significance, $\sigma_{\rm w}$ of each of the input variables, as perceived by the first five neural network models in the committee (Fig. 5f). The neural network permits investigating the effect of each input variable to be analysed individually (Fig. 7b, d, f, h, j), which may be impossible to achieve experimentally. Predictions are ready as per the example shown in Table 1 (YS Model: last column). It is prominent that when the effect of a certain variable is calculated (Fig. 7b, d, f, h, j), others are kept unaltered, which is not possible in real situation; but is important to understand the fundamentals. It is also noted from Fig. 7a, c, e, g and i that there is a tremendous scatter in YS data as a function of its influencing variables. It is to be remembered that other variables are not kept constant here, they are simultaneously operated. Possible 3D graphs (interacting variables) of the entire raw dataset are presented in Fig. 1. Huge scatter is also displayed in these plots (Fig. 1). It may also happen that more variables are interacting in a complex manner during tensile deformation of the alloy. Hence, neural computation has been performed to understand the individual effect of each parameter on YS (Fig. 7b, d, f, h, j). Figure 7b shows that with the increase in NA, the calculated YS decreases sharply. It is seen from Fig. 7d that with the increase in testing temperature, the calculated YS decreases considerably in a linear fashion, which seems to be logical. Figure 7f clearly represents that with the increase in RR, predicted YS drops significantly. Predicted YS increases sharply with the increase in ND (Fig. 7h). The calculated YS values increase with the increase in ESCF (see Fig. 7j). The prediction shown in Fig. 7d has very small error bars and is in the range of the experimentally measured dataset (Table 1). All the error bars manifest the combined

effect of modelling uncertainty $(\pm 1\sigma)$ and noise of the committee model (see Fig. 6a). All these variables influencing YS are approximately linear in nature (Fig. 7b, d, f, h, j). The error bars, therefore, become significantly large when the data are sparse or locally noisy (Fig. 7j – with high value of stress concentration factor).

The deformation and fracture behavior of Ti-8Al-1Mo-1V alloys at various temperatures and notch geometries are thoroughly discussed elsewhere [67]. As the temperature increased, the point of crack initiation progressed towards the axis. Sanyal et al. [31] explained that fracture features change with the notch geometry for the alloy Inconel 625. Wang et al. [88] also explored the influence of ND and notch flank angle on the stress concentration factor employing finite element (FE) simulation and mechanical tests. They found that with increasing ND and notch flank angle, the fracture load and "high stress volume" showed marked variation, but the stress concentration factor remained relatively constant throughout [88]. Concerning the effect of notch geometry on the stress concentration factor, Tetelman et al. [89] evaluated the influence of notch RR on the local cleavage fracture stress concentration factor by means of the slip-line field analysis. The study of Lewandowski and Thompson [90] corroborated that the stress concentration factor of fully pearlitic microstructure was independent of the notch RR introduced. The macroscopic YS of notched specimens of ductile materials are usually higher than those of the unnotched specimens owing to the constraint of plastic flow behaviour. While Bridgman's analysis [91] endorses a correction factor which successfully predicts this increase, the analysis is based on the assumption that yielding occurs uniformly in the specimen cross-section rather than locally to the notch root. In particular, it is worth indicating the study of Creager [92] who generalised the problem of a stress concentrator on the basis of fracture mechanics concepts by accounting for the finite value of notch RR.

The metallurgical significance of the inputs is now analysed (Fig. 6d). The solid mechanics approach has also been taken care of to understand this. The σ_w value represents the extent to which a particular input explains the disparity in the output data, rather like a partial correlation coefficient in a linear regression analysis. The testing temperature on the whole explains a large proportion of variation in YS of

Table 2. Bayesian neural network architecture.

Model Parameters	YS-Model	UTS-Model	TFS-Model	RA-Model
Model type	BNN	BNN	BNN	BNN
Number of models	100	100	100	100
Models successfully trained (decreasing <i>LPE</i>)	93	100	100	100
Suggested models in committee	93	1	2	2
Minimum test error	0.19	0.04	0.15	0.16
Search for maximum noise	0.06	0.02	0.05	0.05
Input, Hidden, Output (best model)	5, 2, 1	5, 2, 1	4, 2, 1	5, 2, 1
Data set	103	103	64	103
Transfer function	tanh	tanh	tanh	tanh
Validation data set	12	12	12	12
Sigma noise	0.3	0.3	0.3	0.3
Random weight	0.3	0.3	0.3	0.3
Initial Weight	0	0	0	0

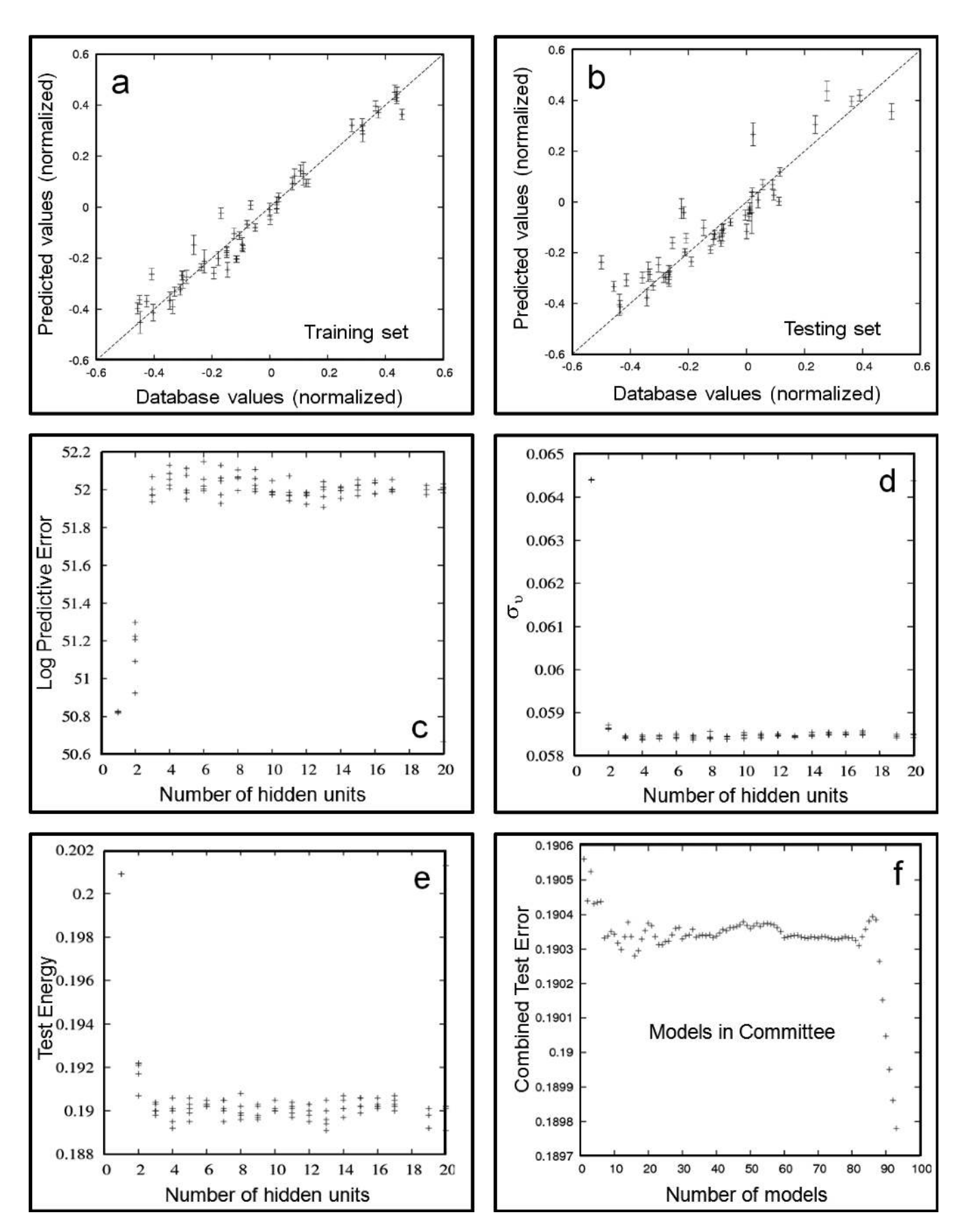


Fig. 5. Modelling results (YS-Model): (a) Training set, (b) Testing set, (c) Log predictive error (LPE) as a function of number of hidden units, (e) Test error (T_e) as a function of number of hidden units, and (f) Combined test error as a function of number of models.

the titanium alloys. The effect of testing temperature on the generation of microstructure for the particular alloy is interpreted in literature [67]. After that, notch RR is featured. All the variables (T > RR > NA > ND > ESCF) considered were found to have significant influence on the output, indicating a good choice of input variables. The rank of each input variables influencing YS is found (model results) in Fig. 6d. However, clear trends (Fig. 7b, d, f, h, j) in predictions are also noted. A large value of σ_w implies that the input concerned explains a relatively large variation in YS in the experimental dataset. The σ_w value is not an indication of sensitivity of the YS to a particular input.

4.2. Tensile strength model

The neural network models (*UTS*-Models) were extensively trained with 103 individual experimentally measured data points, of which a random half of the data formed the training dataset and other half the test dataset (Table 2). The procedures are otherwise identical to those already described for the *YS*-model, resulting in the characteristics illustrated in Fig. 8. The performance of the optimum committee of the best models is shown in Fig. 9a. Details of

one member of the optimum committee are clearly noted in Table 2. Figure 8 describes the entire UTS-Model results. The predictions made using the optimum committee of models are shown in Fig. 10b, d, f, h and j. The use of the UTS-Model is presented in Fig. 9b and c, which indicates that the model behaves robustly for unseen experimental data. Figure 9d also compares the significance, $\sigma_{\rm w}$ of each of the input variables, as perceived by the best model, which will be discussed later.

Significant scatter is noticed from the possible 3D graphs in Fig. 2 and 2D graphs in Fiog. 10a, c, e, g and i. It is probable that there might be other complex interactions too, which are unknown. After neural computation, a convincing trend is achieved (see Fig. 10b, d, f, h, j). Predictions are ready as per the example shown in Table 1 (*UTS*-Model: last column). It has been found from Fig. 10b that with the increase in *NA*, the calculated *UTS* values are decreasing sharply in a linear fashion. From Fig. 10d, it is noted that with increase in testing temperature, the predicted *UTS* decreases sharply. The calculated *UTS* values decrease drastically in a linear fashion (Fig. 10f) with the increase in notch *RR*. The error bars' length is also noted here (Fig. 10f). Figure 10h convincingly indicates that with the

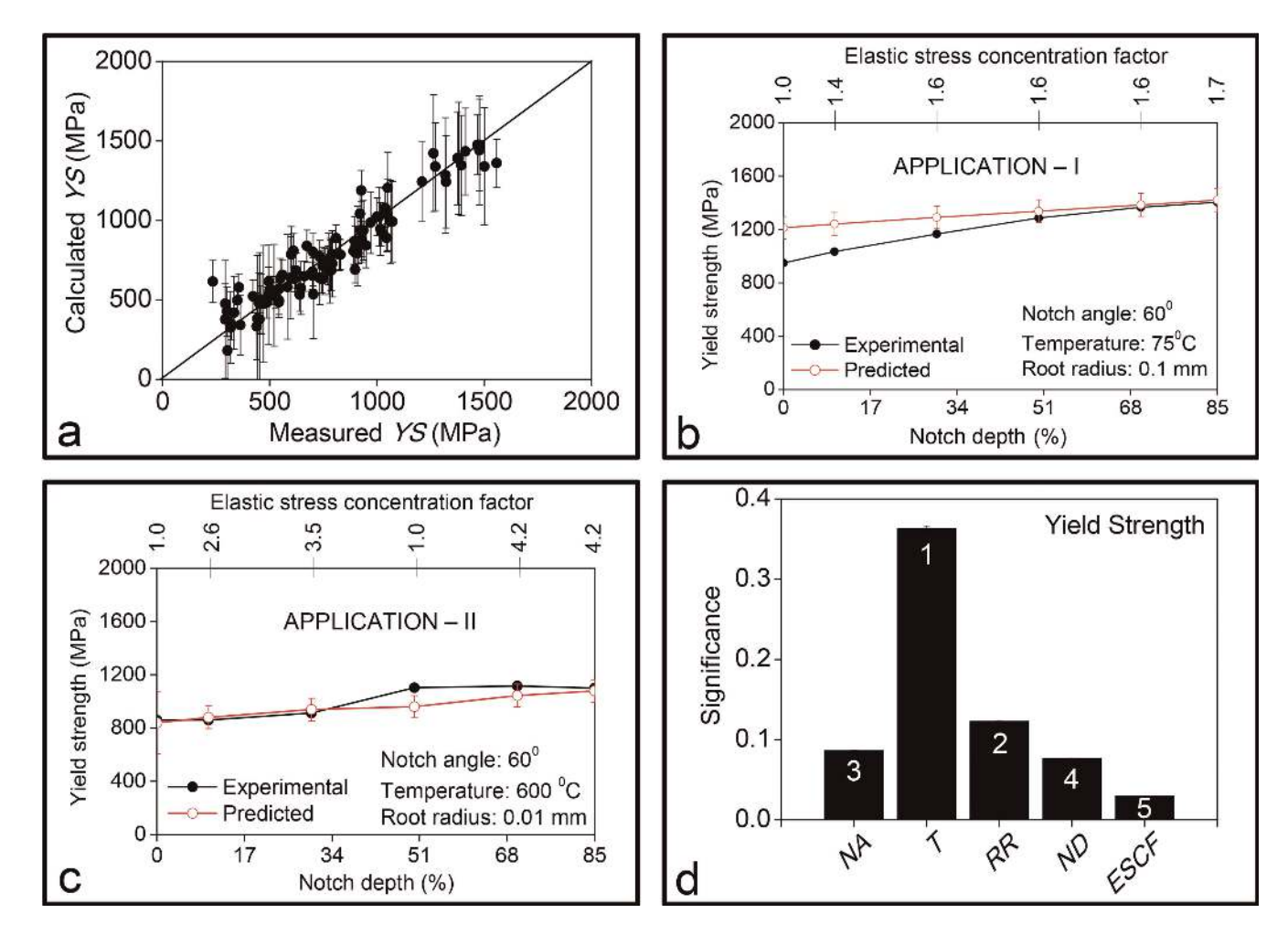


Fig. 6. (a) Training data for the best committee model (training was done on the whole dataset) for YS prediction, (b) Application – I: Comparison of measured and calculated YS as a function of ND and ESCF, where other variables ($NA = 60^{\circ}$, $T = 75^{\circ}$ C, RR = 0.1 mm) are kept constant, (c) Application – II: Comparison of measured and calculated YS as a function of ND and ESCF, where other variables ($NA = 60^{\circ}$, $T = 600^{\circ}$ C, RR = 0.01 mm) are kept constant, and (d) Significance, $\sigma_{\rm w}$ of each input variable as perceived by five neural network models in committee, in influencing YS. These application data (source [67]) were unseen by the model.

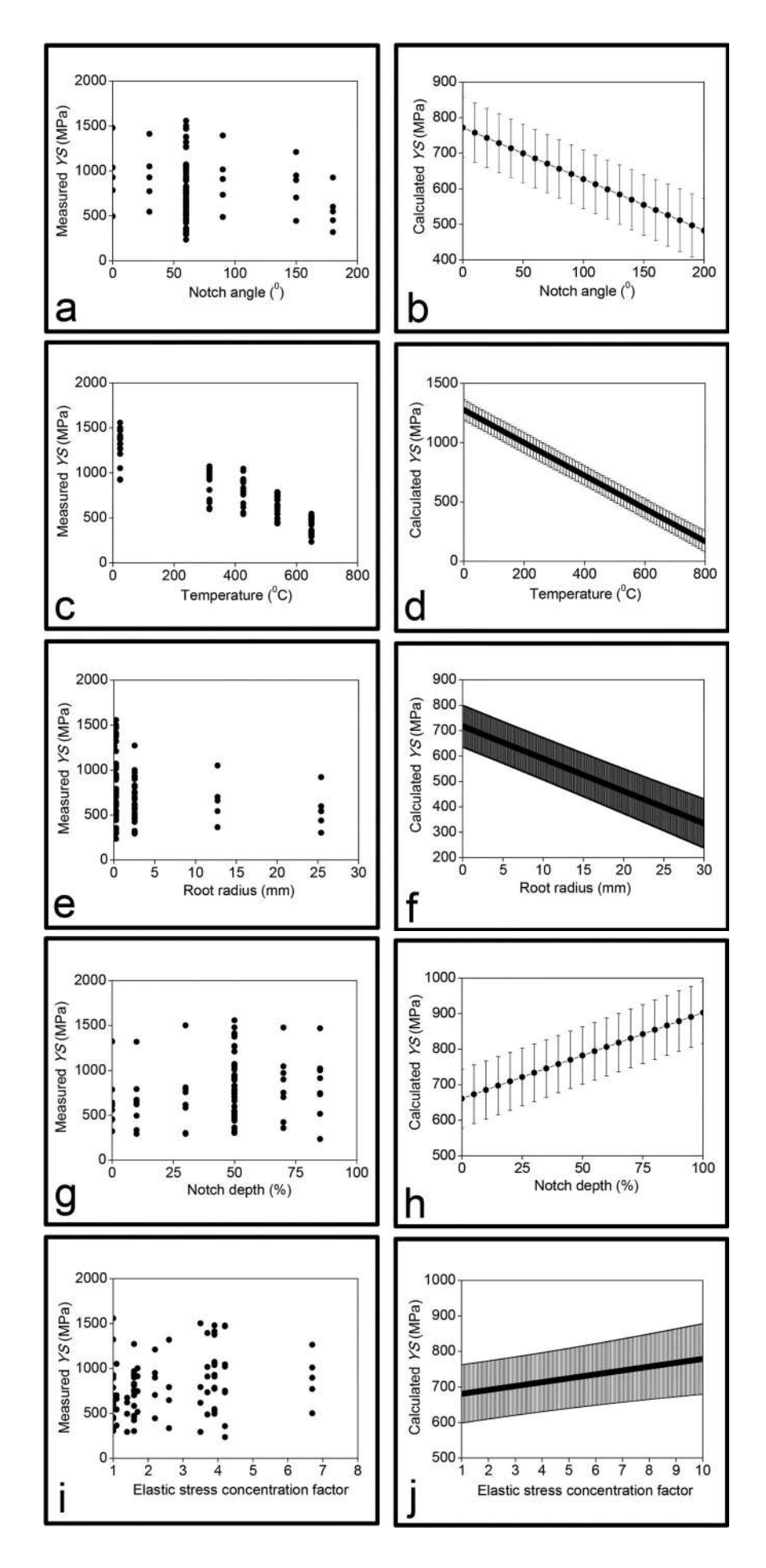


Fig. 7. Comparison of experimentally measured and model calculated YS data of Ti-8Al-1Mo-1V alloy in 2D plots as a function of (a, b) NA, (c, d) T, (e, f) RR, (g, h) ND and (i, j) ESCF. Note: in experimentally measured graphs (a, c, e, g and i), all influencing variables are interacting with each other and in the model predicted graphs (b, d, f, h and j), other variables are kept unaltered (see Table 1: YS-Model database according to 'example' column).

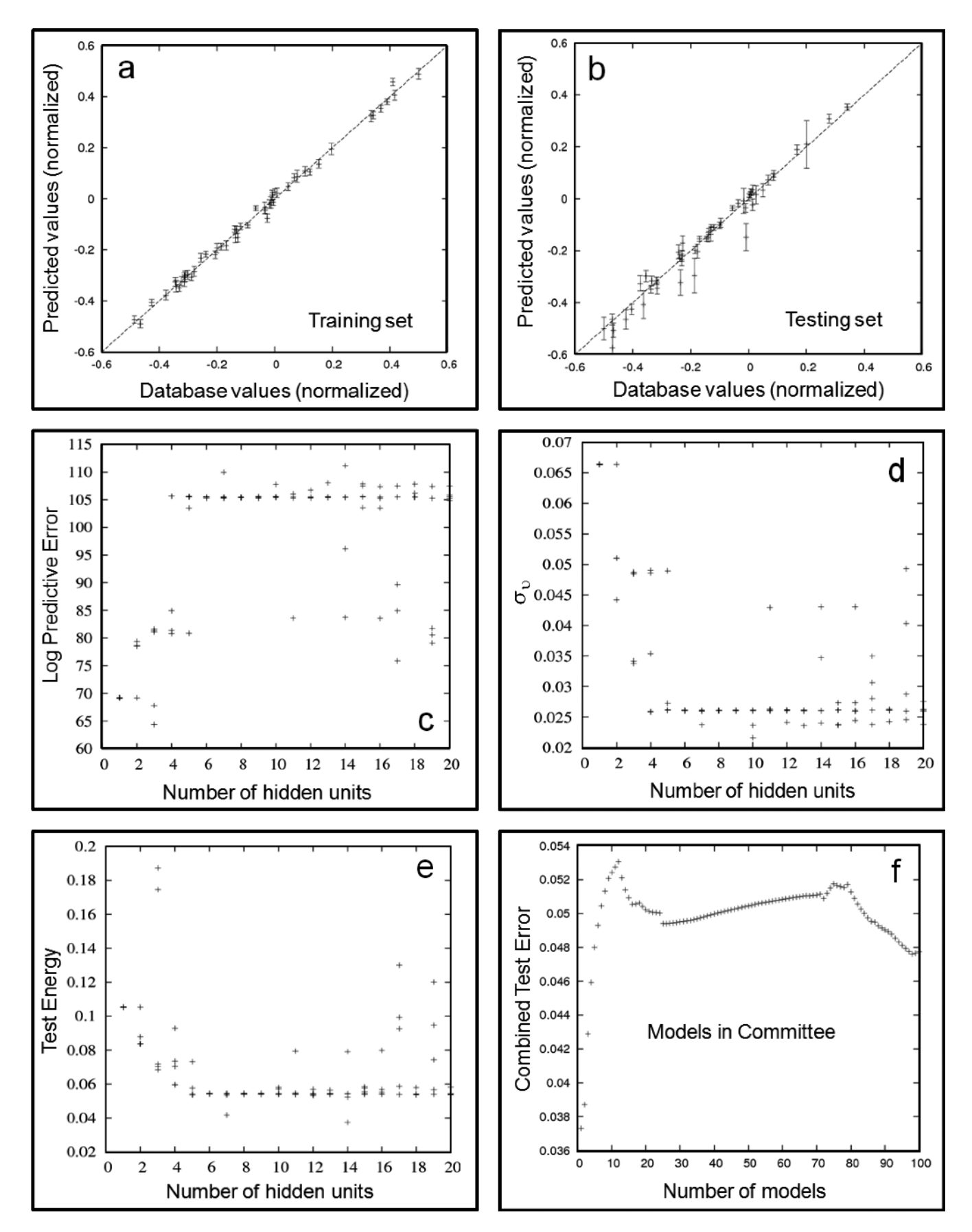


Fig. 8. Modelling results (*UTS*-Model): (a) Training set, (b) Testing set, (c) Log predictive error (*LPE*) as a function of number of hidden units, (d) $\sigma_{\rm v}$ as a function of number of hidden units, (e) Test error ($T_{\rm e}$) as a function of number of hidden units, and (f) Combined test error as a function of number of models.

increase in *ND*, calculated *UTS* values increase sharply. From Fig. 10j, it is clear that with increase in *ESCF*, the predicted *UTS* values increase. This is expected since the *UTS* values are measured at large plastic strains whereas *YS* are more sensitive to the initial microstructure of the alloy. The microstructural interpretations for this alloy are readily discussed in Ref. [67].

Depending on whether the nominal UTS in the notched specimen is higher or lower than in unnotched specimens, materials are classified as being notch ductile or notch brittle, respectively as explained in literature [93]. The more difficult issue of yielding in notched specimens has received very little attention (Kochendorfer et al. [94]; Dietmann [95]; Backsch et al. [96]). Hence, the value of results generally available from a notch tensile test [67] to be found in comparing different materials rather than in generating data which can be used for engineering design purposes. Lubahn [97] goes so far as to state that the useful applicability of the information extracted from the notch tensile experiments is so limited as to be almost useless for many structural engineering purposes. Additional geometrical notch induces a non-linear stress field surrounding it (explained in Fig. 10 [16]). As a result of interaction between microstructure and mechanical conditions of the alloy, favourable local sites of plastic instability may occur. They may quantitatively differ depending on the external condition of the notch, such as size and shape as has been observed during mechanical experiments. Hahner et al. [98] reported that the phenomena for non-uniaxial specimens must take into account the geometrical notch effects in addition to the standard model.

Crucial and precious experimental data have shown that the *UTS* values of composite laminates are severely reduced by the presence of a stress concentration in the form of a crack/hole, which has been documented in Refs. [99, 100]. This appears to be related to the brittleness of the fibers employed in advanced critical applications. Metals generally yield, making the presence of a stress concentration less severe. Oyane et al. [101] researched compressive plastic constitutive equations of porous materials with consideration of the hydrostatic pressure and suggested that the density of material decreases during deformation and that fracture occurs when the density of material reaches a certain critical value. The present author has already experimented and proved this issue for AISI 304 LN stainless steel under tensile deformation at various strain rates [36]. However, it

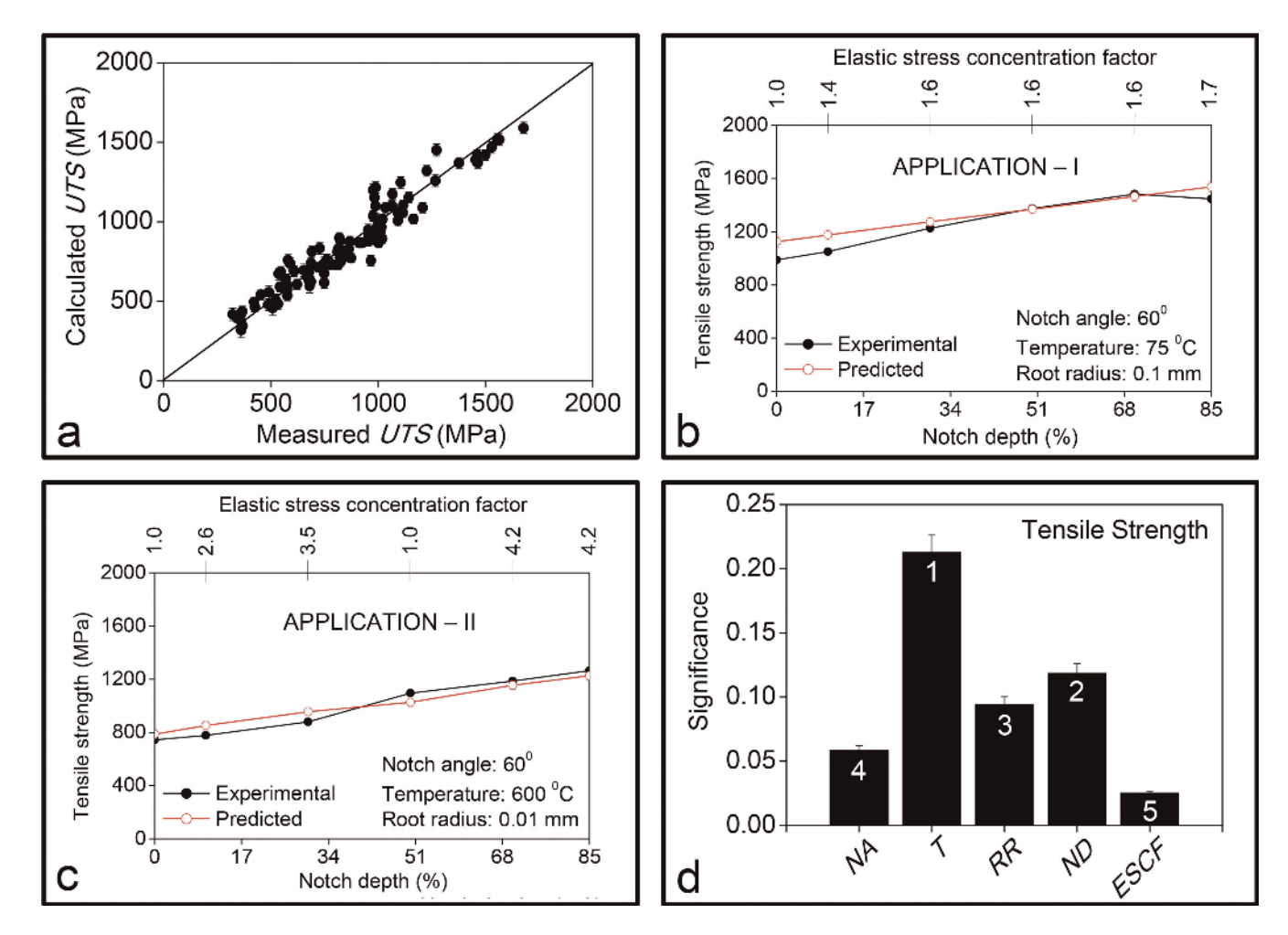


Fig. 9. (a) Training data for the best committee model (training was done on whole dataset) for *UTS* prediction, (b) Application – I: Comparison of measured and calculated *UTS* as a function of *ND* and *ESCF*, where other variables ($NA = 60^{\circ}$, $T = 75^{\circ}$ C, RR = 0.1 mm) are kept constant, (c) Application – II: Comparison of measured and calculated *UTS* as a function of *ND* and *ESCF*, where other variables ($NA = 60^{\circ}$ C, RR = 0.01 mm) are kept constant, and (d) Significance, σ_{w} of each input variables as perceived by five neural network models in committee, in influencing *UTS*. These application data (source [67]) were unseen by the model.

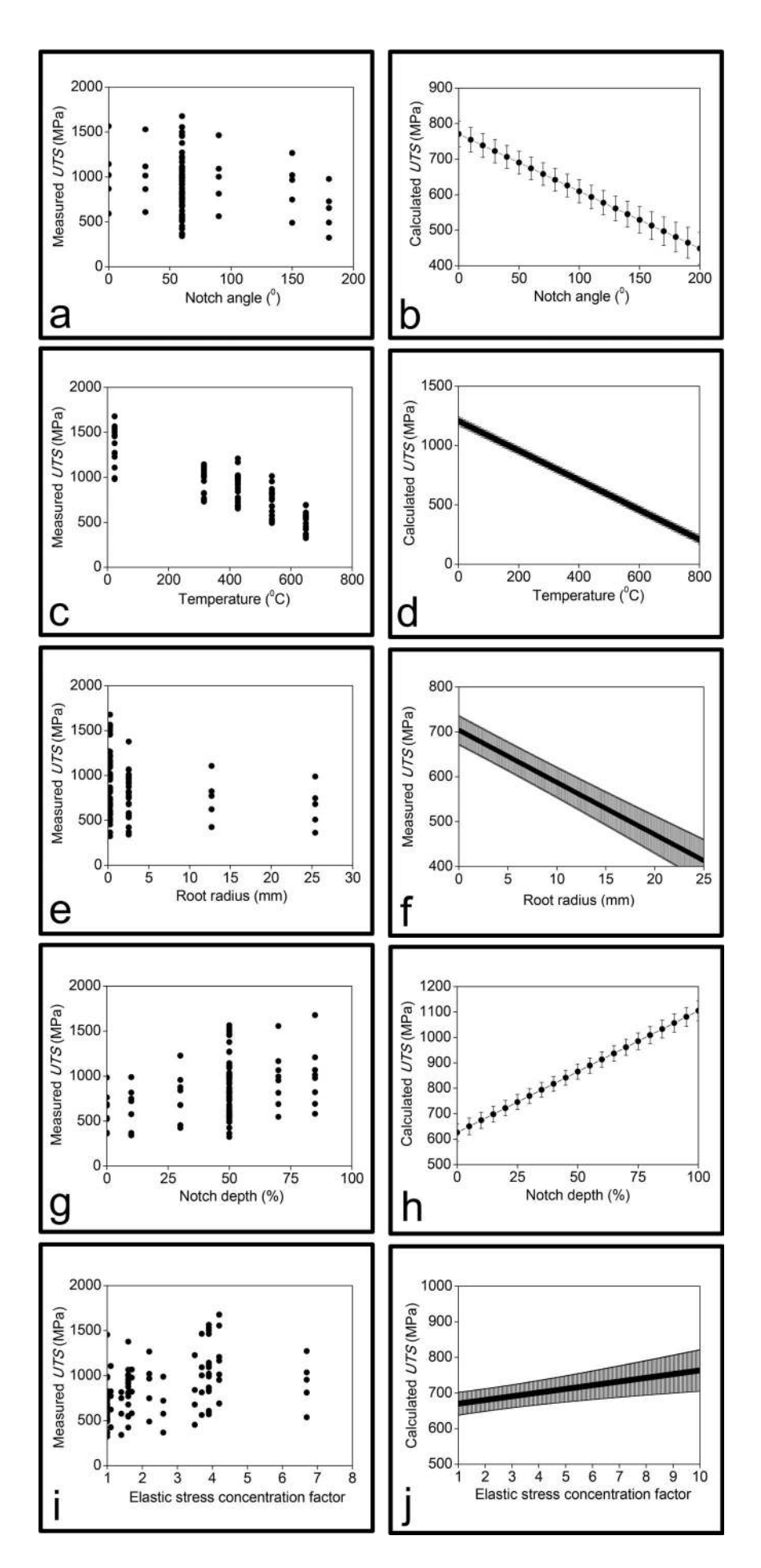


Fig. 10. Comparison of experimentally measured and model calculated *UTS* data of Ti-8Al-1Mo-1V alloy in 2D plots as a function of (a, b) *NA*, (c, d) *T*, (e, f) *RR*, (g, h) *ND*, and (i, j) *ESCF*. Note: in experimentally measured graphs (a, c, e, g and i), all influencing variables are interacting with each other and in the model predicted graphs (b, d, f, h and j), other variables are kept unaltered (see Table 1: *UTS*-Model data according to 'example' column).

is to be kept in mind that under notch tension, the stress is not uniform anymore [32]. There are stress concentrations around the notch root and also a negative stress gradient formation as increasing distance away from the notch roots, which has been reported in literature [32, 102]. The uniform tensile stress-state in unnotched specimens and work-hardening ability of the alloys make plastic deformation of dislocation slipping homogeneously distributed over the whole gauge length of the specimen, and finally a large tensile plasticity is gained [102]. It is well known that in the region of a notch, stress concentration is increased compared to that in material beyond it. Additionally the stress-state becomes triaxial instead of uniaxial, as explained by Majima et al. [103]. For both non-dimensional groups, with all parameters fixed except for bar size, Needleman [104] found that for sufficiently small bars, the notch triggers necking, whereas for sufficiently large bars necking ultimately occurs away from the notch. The transition from notch induced necking to notch ignoring necking depending on the size and is driven by the material inertia [104].

The perceived significance of a single model is already presented in Fig. 9d. In this case also, testing temperature features prominently and after that comes notch diameter. All the variables (T > ND > RR > NA > ESCF) considered were found to have a significant effect on the output, indicating a good choice of inputs. The rank of each variable influencing UTS is shown in this figure. The microstructural interpretations with the notch geometries and testing temperature are fully discussed in Ref. [67].

4.3. Fracture strength model

The true fracture stress (TFS) for a notched specimen is defined as the fracture load divided by original cross-sectional area at the notch, i.e., net fracture stress value. If there is no notch effect, the fracture stresses for notch-free and notched specimens must be the same. The models were trained by 64 individual experiments, of which a random half of data formed the training and the other half a testing dataset (see statistics in Tables 1 and 2). The model consists of four input variables (Table 2). The modelling procedures are otherwise identical to those explained earlier, resulting in the characteristics illustrated in Fig. 11. Figure 11 describes the entire TFS-Model results. The training, test, LPE [71– 74] associated with each of the 100 models created are clearly explained in Fig. 11. The performance of the optimum committee of the best model is elucidated in Fig. 12a. Details of two members of the optimum committee are shown in Table 2. Application of the model for unseen data is manifested in Fig. 12b and c which displays a reasonably good match between the measured and calculated TFS data. Figure 12d compares the significance, $\sigma_{\rm w}$ of each of the input variables, as perceived by the best model, which will be discussed in detail later.

Figure 13a, c, e and g shows the scatter of *TFS* data as a function of particular variables for the alloy, where other influencing variables are operated in the practical service conditions. Complex interactions of fracture stress with other variables in three dimensions are also presented in Fig. 3. The interactions are unknown and highly complex, which can happen with multiple variables together during tensile deformation. Predictions are ready as per the example shown in Table 1 (*TFS* Model: last column). It is appar-

ent from Fig. 13b that with the increase in testing temperature, calculated TFS remains almost constant up to $\approx 400\,^{\circ}\text{C}$ and beyond that there is a drastic decrease in TFS data. The error bars' lengths are also noted, which was explained earlier. With the increase in RR, there is a slight drop in the predicted TFS values (Fig. 13d). It has been noticed from Fig. 13f that with the increase in ND, calculated TFS values increase in an exponential manner, where the other variables are kept unaltered. From Fig. 13 h, it is convincingly understood that with the increase in ESCF, the calculated TFS decreases a little. Long error bars are also featured here.

Tensile fracture often occurs once a shear band pierces the tensile specimen. However, in crystalline solids, multiple slip-bands would be produced due to the very low energy density threshold for initiation [16]. The interactions between dislocations and other defects, like point defects (e.g., solute atoms, interstitial atoms, clusters, vacancies etc.), line defects (e.g., dislocations), planar defects (e.g., grain boundary, phase boundary, phase interfaces, slip bands, twin bands etc.), and volumetric defects (e.g., inclusions, second phase particles, porosity etc.) would essentially contribute to the work-hardening ability of the materials, which causes the plastic deformation to distribute homogeneously over the whole gauge length of the tensile specimen rather than localising into several single slipbands [16]. In a notched specimen, the stress concentration around notch root greatly increases the local stress level, which leads to a final fracture of the specimen at a lower nominal stress [16]. The authors of [60] have found that the geometrical notch has an effect on the formation of shear bands on the surfaces of the specimen. It supplements the results obtained by Graff et al. [105, 106] with a quantitative analysis of stress-strain curves and of the crucial role played by the notch dimensions. From the tensile fractographs of Ti-8Al-1Mo-1V alloy, it has been interpreted that embrittlement effects associated with stress triaxiality were more predominant in the 85 % ND specimens than in those with shallower notches [67]. Furthermore, fully developed triaxiality conditions pertained at lower temperatures for specimens with deeper notches. At higher temperatures, the position of initiation of fracture and its mode of crack propagation are more dependent on the test temperature than specimen geometry. It is apparent that both the stress system and the testing temperature affect crack nucleation and propagation for Ti-8Al-1Mo-1V alloy [67].

The perceived significance of the two models is shown in Fig. 12d. In this case also, testing temperature featured prominently and after that, notch diameter is featured. All the variables (T > ND > RR > ESCF) considered were found to have a significant effect on the output, indicating a good choice of inputs for the model. It is clearly noted that the effect of notch RR and ESCF are being minimum compared to others.

4.4. Ductility model

Naturally, strength alone is not a sufficient indicator of deformation and fracture behaviour of materials. Ductility and toughness must also meet the design specifications. Ductility-limits and variability are of particular concern in the design of components/structures having notches or other stress concentrators, where plastic flow may not be

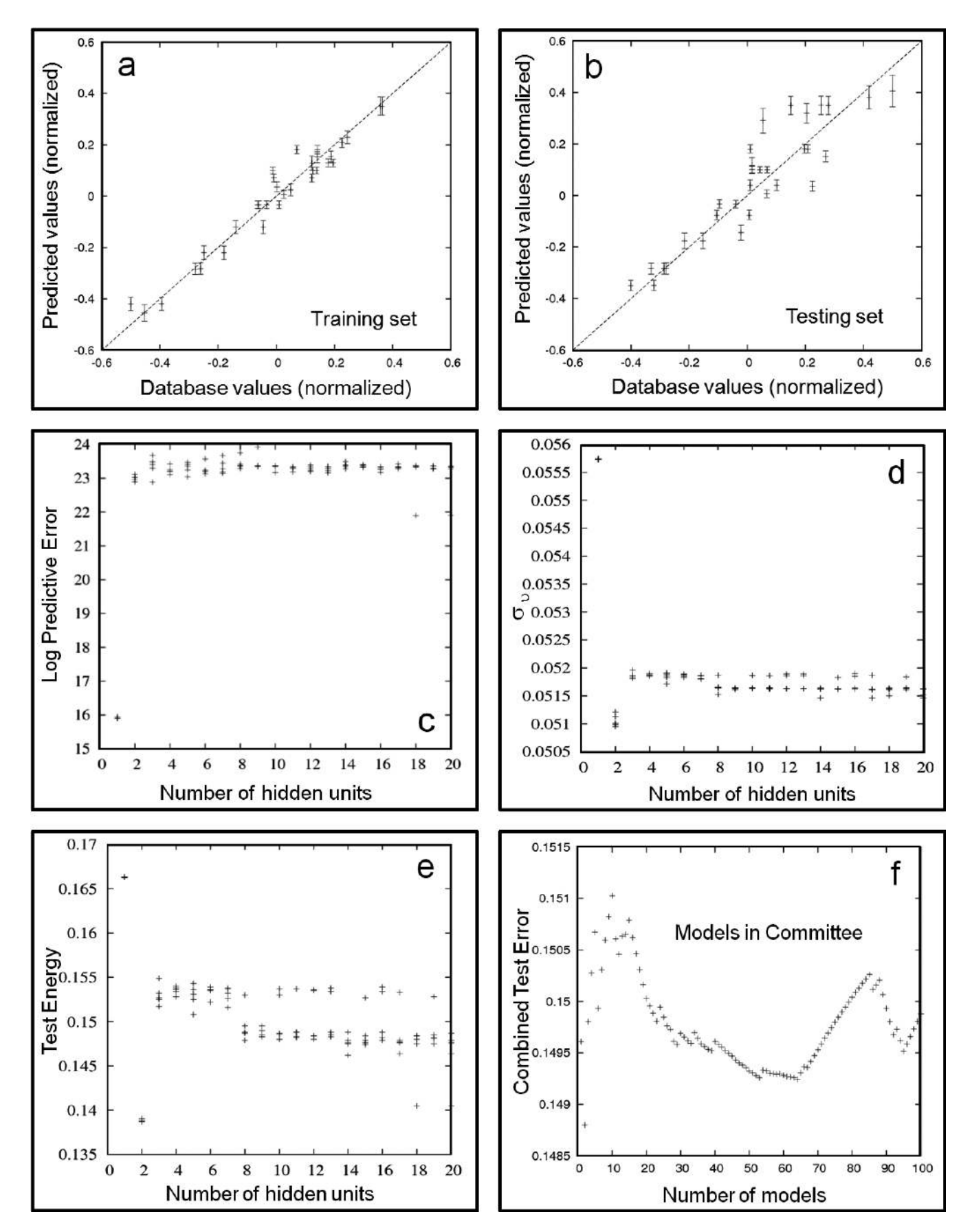


Fig. 11. Modelling results (*TFS*-Model): (a) Training set, (b) Testing set, (c) Log predictive error (*LPE*) as a function of number of hidden units, (d) $\sigma_{\rm v}$ as a function of number of hidden units, (e) Test error ($T_{\rm e}$) as a function of number of hidden units, and (f) Combined test error as a function of number of models.

sufficient to reduce the large stress concentrations [107]. Ductility is a great concern at stress concentrators, where the material may not be able to experience sufficient plastic flow to blunt the stress concentrations [108]. Knaul et al. [108] have shown that notched specimens subjected to monotonic loading would experience higher failure strains than unnotched specimens. In the exhaustive experiments performed by Knaul et al. [108], there is a trend of increasing maximum strains at failure seen in test specimens as the volume of highly strained material is decreased. This apparent size effect suggest that failure strains acquired from the mechanical tests on large unnotched specimens will provide a lower bound on maximum strains seen in the notched components [108].

In the current research, neural network models are developed for *RA* to understand the notch geometry and temperature effects on it. The model consists of 5 inputs listed in Tables 1 and 2, which are often considered to influence the ductility. The specimen geometry and testing temperature determine the fracture properties of the material. A total 103 individual experimental data were gathered systematically from the literature [67]. Figure 14 elucidates the entire *RA*-Model results. The modelling procedures are similar to

those as explained earlier. The training, test, LPE [71–74] associated with each of the 100 models are clearly illustrated in Fig. 14. From all the 100 models, a committee of two best models was found to give the lowest test error; each member of the committee (Fig. 14f) was then retrained on the entire dataset to create the final committee model (Fig. 15a). The application of the committee model is presented in Fig. 15b and c, which displays reasonably good match between the measured and calculated RA. Figure 15d compares the significance, $\sigma_{\rm w}$ of each of the input variables, as perceived by the best model.

By employing the committee model (Fig. 15a), the predictions (Fig. 16b, d, f, h and j) are made. Predictions are ready as per the example shown in Table 1 (RA Model: last column). It is seen from Fig. 16a, c, e, g and i that there is a huge scatter in RA data as a function of its influencing parameters, where other variables are interacting with each other with reasonable complexity. For comprehending such complex interactions, possible 3D graphs are already sketched in Fig. 4. Neural computation has been successfully employed to get rid of such complexity and to see the convincing trends of RA with respective parameters, where other variables are kept constant. With the increase in NA,

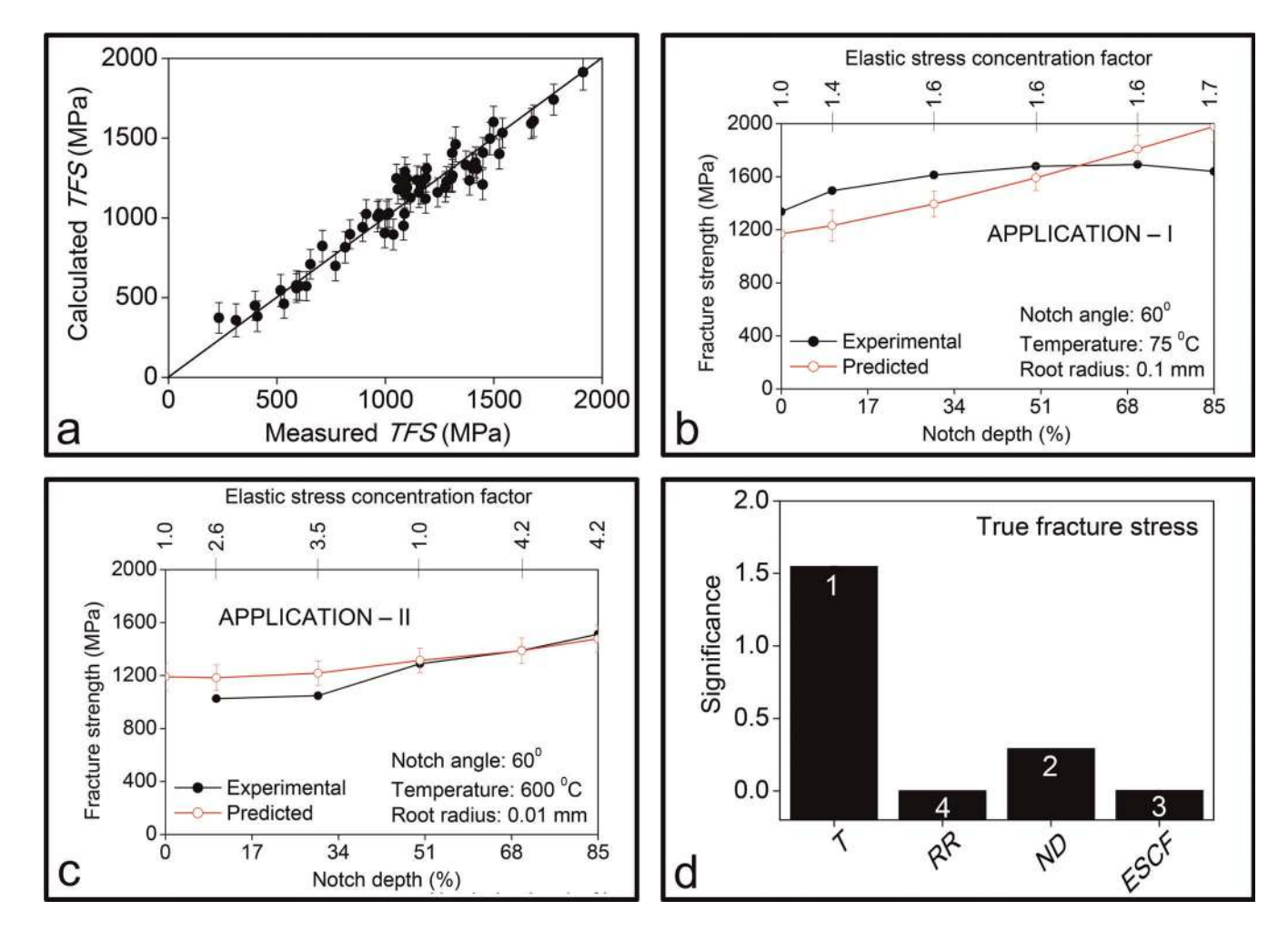


Fig. 12. (a) Training data for the best committee model (training was done on the whole dataset) for *TFS* prediction, (b) Application – I: Comparison of measured and calculated *TFS* as a function of *ND* and *ESCF*, where other variables ($NA = 60^{\circ}$, $T = 75^{\circ}$ C, RR = 0.1 mm) are kept constant, (c) Application – II: Comparison of measured and calculated *TFS* as a function of *ND* and *ESCF*, where other variables ($NA = 60^{\circ}$, $T = 600^{\circ}$ C, RR = 0.01 mm) are kept constant, and (d) Significance, $\sigma_{\rm w}$ of each input variables as perceived by five neural network models in committee, in influencing *TFS*. These application data (source [67]) were unseen by the model.

calculated RA decreases a little up to $\approx 55\%$ and beyond that it again increases (Fig. 16b). This seems to be logical as per the existing solid mechanics theories. At the initial values of NAs (below 40% and above 60%) there are uncertainties in predictions. In these regimes, large error bars are noted (Fig. 16a). This means that the availability of experimental data were limited in these ranges. Hence, new and systematic experiments in these ranges are encouraged for future research. It has been found from Fig. 16d that with the increase in testing temperature, calculated RA increases

in an approximately exponential manner. With the increase in notch RR, calculated RA decreases drastically and after 10 mm-RR, there is uncertainty in prediction (Fig. 16f). With the increase in ND, the calculated RA decreases up to 75% and beyond that it is almost saturated (Fig. 16h). Figure 16j shows that with the increase in ESCF, the calculated RA decreases sharply. The sharper the notch, the lower would be the ductility. Ductility decreases as the stress triaxiality increases. Anderson [109] indicated that, notwithstanding, the ductile fracture toughness is simply size

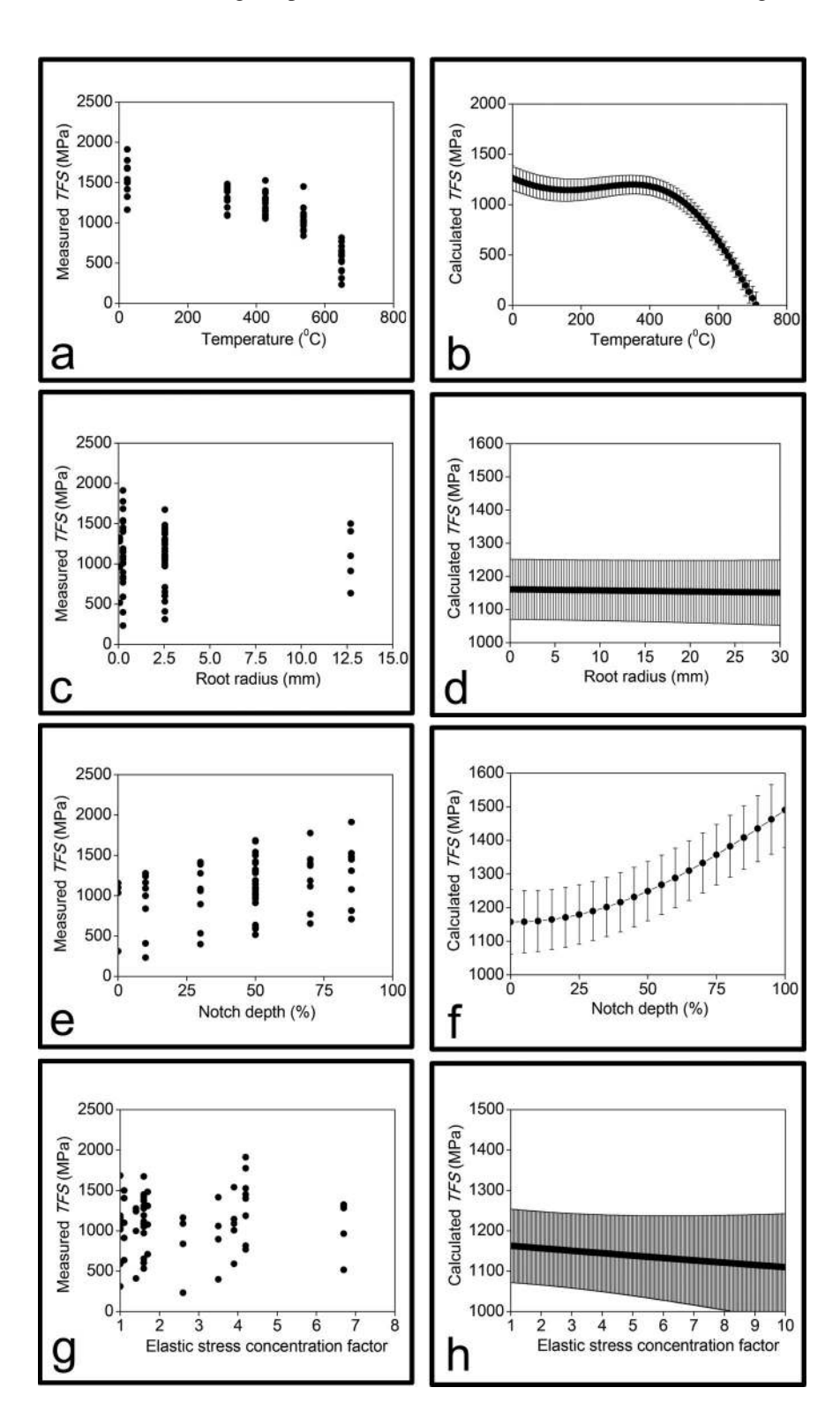


Fig. 13. Comparison of experimentally measured and model calculated *TFS* data of Ti-8Al-1Mo-1V alloy in 2D plots as a function of (a, b) *T*, (c, d) *RR*, (e, f) *ND*, and (g, h) *ESCF*. Note: in experimentally measured graphs (a, c, e and g), all influencing variables are interacting with each other and in model predicted graphs (b, d, f and h), other variables are kept unaltered (see Table 1: *TFS*-Model database according to 'example' column).

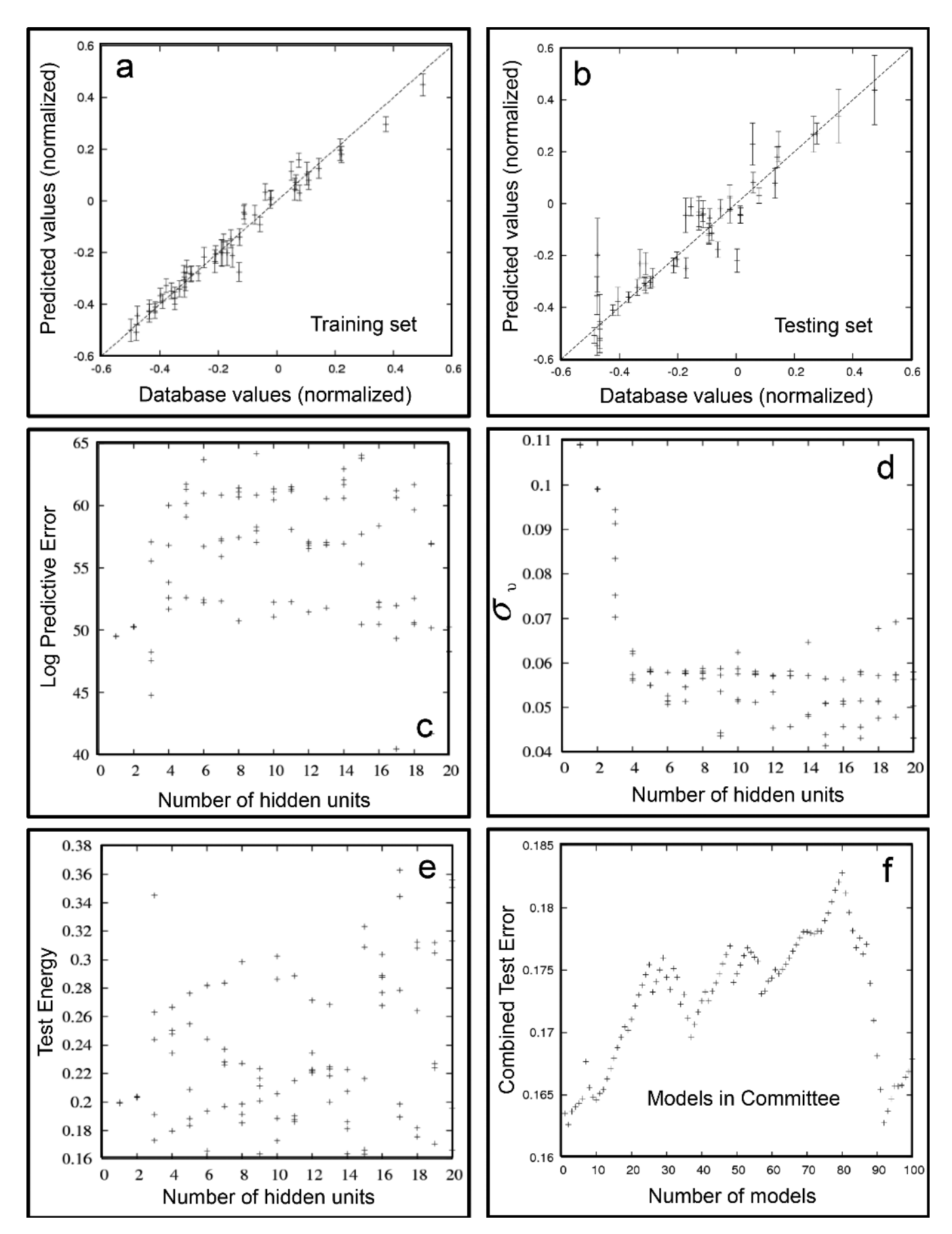


Fig. 14. Modelling results (*RA*-Model): (a) Training set, (b) Testing set, (c) Log predictive error (*LPE*) as a function of number of hidden units, (d) σ_v as a function of number of hidden units, (e) Test error (T_e) as a function of number of hidden units, and (f) Combined test error as a function of number of models.

dependent in panel loaded under tension; the size dependence is not nearly as severe as it is for cleavage fracture. It has been shown by Sui et al. [110] that the presence of sharp notches decreased the strength and ductility of copper. The fracture mode was found to be independent of notch acuity and test conditions [110]. Notch acuity dependence seems to be the dominant effect on this value and the trend is same for UTS [110]. The uniform elongation (ε_n) decreases sharply from the uniaxial to multiaxial state and then increases slightly with the increase in notch acuity [110]. When the notch acuity is given, the model (by Sui and Sandström) gives almost the same ε_u despite of varying strain rates and temperature [110]. Although the ε_u values measured at different temperatures and strain rates are not identical, the differences are adequate. The presence of a notch decreased the UTS, elongation and RA [110].

Notched tensile experiments performed by Knaul et al. [108] also indicate that the cast Ti-47.9A1-2.0Cr-2.0Nb alloy exhibits notch strengthening, where maximum strains at failure in notched specimens were, on average, larger than strains at failure in uniaxial tensile (unnotched) specimens. Increases in maximum failure strains (ε_f) correlated well with the estimated decrease in the volume of material subjected to large strains, suggesting a size effect [107]. Finite element

(FE) predictions for notched tensile specimens and the Neuber design criterion are essentially used to quantify relationships between the tensile ductility, the ability to reduce local stress concentrations through plastic flow, and ultimate failure loads in notched components [108]. Generally, higher stress is required to deform the alloy in the notched specimens although the registered force is lowered compared to the specimen without a notch [111]. This is due to the reduction of cross-section and smaller surface area from where the stress is estimated. In addition, as a result of the geometrical notch, total elongation is much lower than that in the specimen without a notch.

Figure 15d describes the significance, $\sigma_{\rm w}$ of each input variable. In this case also, testing temperature featured prominently and after that elastic stress concentration factor is seen. All the variables (T > ESCF > ND > NA > RR) considered were found to have a significant influence on the output, indicating a good choice of inputs.

5. Conclusions

Tensile properties of titanium alloys as a function of notch geometry and temperature have been analysed using artificial intelligence within a popular Bayesian computational

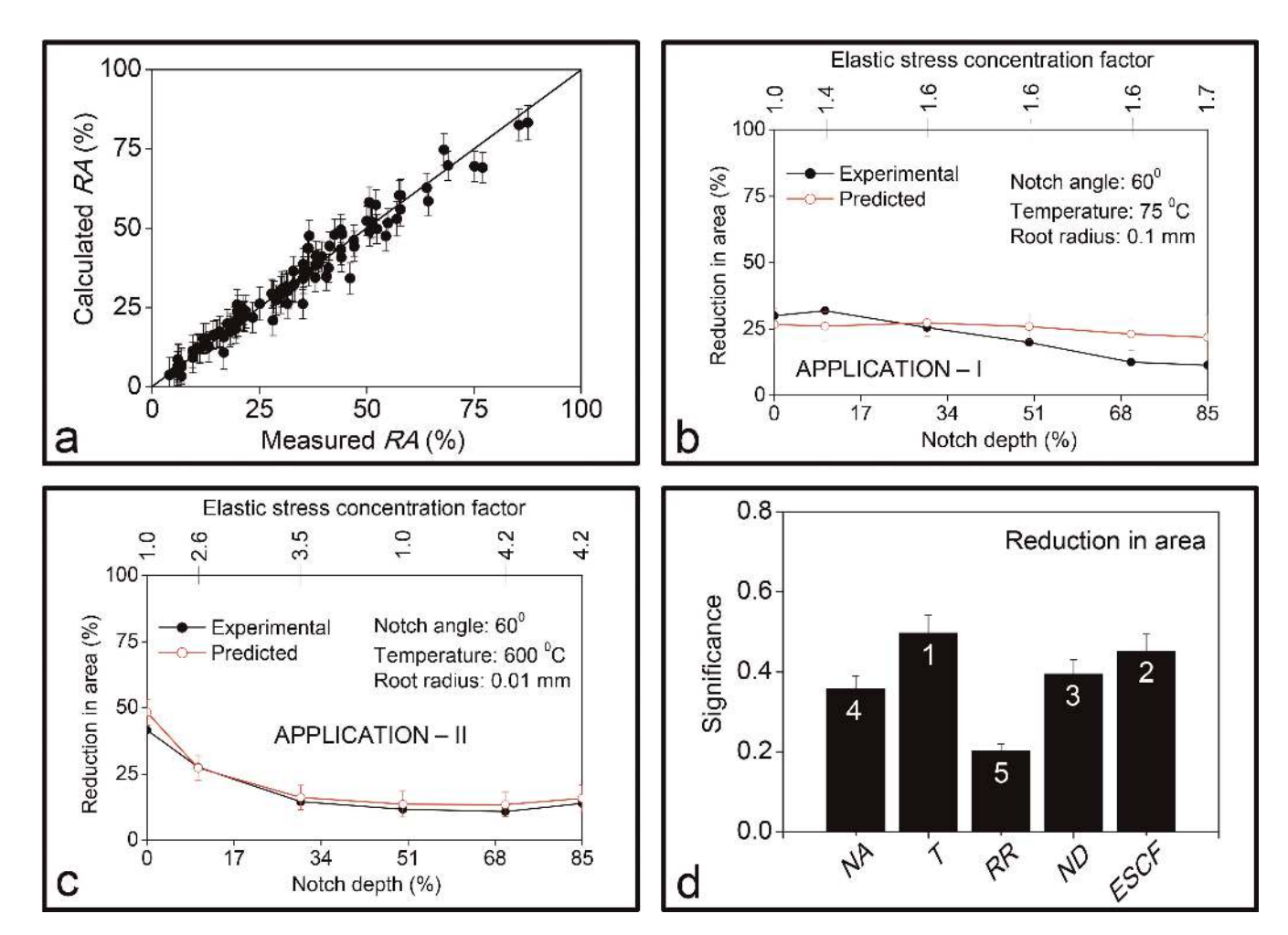


Fig. 15. (a) Training data for the best committee model (training was done on whole dataset) for RA prediction, (b) Application – I: Comparison of measured and calculated RA as a function of ND and ESCF, where other variables ($NA = 60^{\circ}$, $T = 75^{\circ}$ C, RR = 0.1 mm) are kept constant, (c) Application – II: Comparison of measured and calculated RA as a function of ND and ESCF, where other variables ($NA = 60^{\circ}$, $T = 600^{\circ}$ C, RR = 0.01 mm) are kept constant, and (d) Significance, σ_{w} of each input variables as perceived by five neural network models in committee, in influencing RA. These application data (source [67]) were unseen by the model.

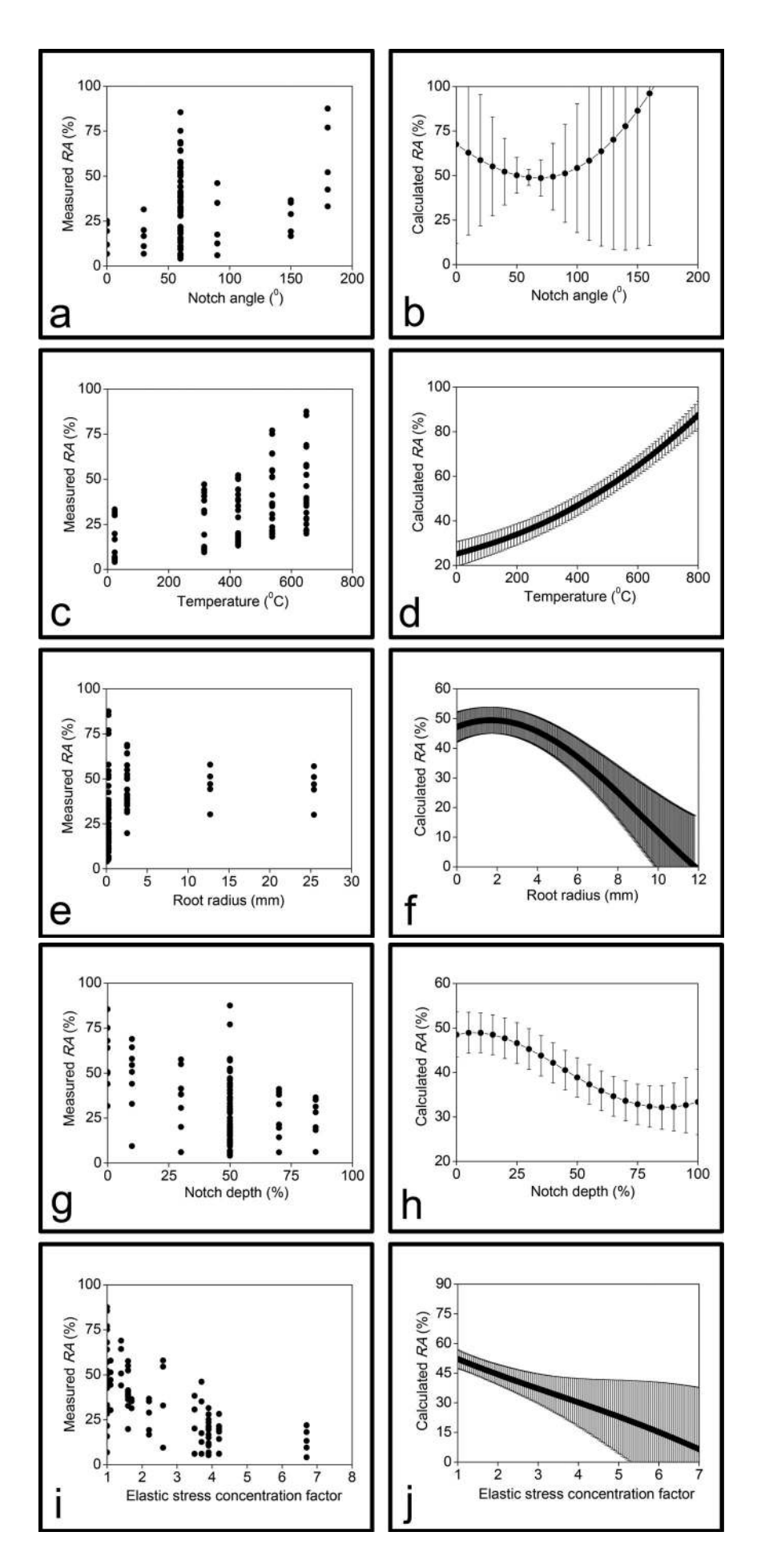


Fig. 16. Comparison of experimentally measured and model calculated *RA* data of Ti-8Al-1Mo-1V alloy in 2D plots as a function of (a, b) *NA*, (c, d) *T*, (e, f) *RR*, (g, h) *ND* and (i, j) *ESCF*. Note: in experimentally measured graphs (a, c, e, g and i), all influencing variables are interacting with each other and in model predicted graphs (b, d, f, h and j), other variables are kept unaltered (see Table 1: *RA*-Model database according to 'example' column).

framework. The experimental data used were essentially obtained from the published literature, which represents a wide variation of notch geometries and testing temperatures to the tensile properties of titanium alloys [67]. The current analysis and previously published experimental results by Jenkins and Willard [67] indicate that the notch geometry affects both the strength and ductility properties of the material, and this notch-effect depends not only on the material itself but also on the associated stress concentration factors. From the macroscopic point of view, the blunt notch specimens of these alloys seem to present "ductile" fracture behaviour, while the acute crack/notch specimens present "brittle" fracture behaviour.

The current model results are summarised briefly. It has been found that with the increase in NA, T and RR; both YS and UTS decrease drastically; on the other hand with increase in ND and ESCF; both YS and UTS increase. The significances of parameters (ranks) in determining YS and UTS of the alloy are in sequences of T > RR > NA > ND > ESCFand T > ND > RR > NA > ESCF respectively. With the increase in T, TFS remains almost constant up to $\approx 400\,^{\circ}\text{C}$ and beyond that it decreases. TFS values remain almost constant with RR and increase drastically with ND. As ESCF increases, TFS decreases a little. The significance of parameters in determining TFS of the alloy are in a sequence of T > ND > ESCF > RR. Lastly, it has been found that with increase in NA, RA decreases a little and beyond a certain angle, it again increases. As T increases, RA increases dramatically. With the increase in RR, ND and ESCF; RA is found to decrease significantly. The significance of input parameters in determining RA of the alloy is in a sequence of T >ESCF > ND > NA > RR. All the models successfully reproduce the experimentally observed trends.

Trends predicted by the present models emerge to be consistent with those expected by the metallurgical and solid mechanics approaches, although it must be emphasised that only the simplest of trends have been examined since the number of variables involved is less. The models can be applied widely because the calculation of error bars whose magnitude depends on the local position in the input space is an inherent feature of the neural network used. The error bar is not simply an estimate of the perceived level of noise in the output values but also includes an uncertainty associated with fitting the function in the local region of the input space. This means that the technique is less dangerous in extrapolation or interpolation since it effectively warns when the experimental data are lacking or exceptionally noisy. The small error bars indicate that the scatter in the database is very small and the large error bars suggest a lack of sufficient data in the range examined, where further experiments may be required. The work has clearly identified the regions of the input space where further experiments should be encouraged. The implication of these findings will be helpful in fundamental understanding of ductile fracture of fcc alloys.

The present author's experience of the neural network analysis suggests that it has considerable potential for useful applications in the fields of solid mechanics and materials science. The maximum possible variables responsible for mechanical properties of titanium alloys have already been included in the current framework of neural computation from the mechanistic point of view and they have been critically reviewed and comprehensively discussed in this

article. There are other variables also responsible for different mechanical properties of titanium alloys. Nevertheless, the current neural network can be created more effectively in discovering better trends while ignoring the noise in the experimental data with a sufficiently larger database. Therefore, there is scope for further research in order to broaden the sensitivity analysis and generalising for other materials also using a larger and comprehensive database including other important input variables such as grain size, initial microstructure/texture, strain rate, chemistry etc., which could be generated by suitable experimentation and thorough literature search.

This information in itself is valuable and would not have been revealed without the Bayesian computational framework under artificial intelligence paradigm. This research will enormously help researchers to understand where further experiments would be required to optimise the strength and ductility of titanium alloys by altering the microstructure and mechanics of the components, which is a challenging task in these days.

I am extremely grateful to Professor Sir H.K.D.H. Bhadeshia, Phase Transformation & Complex Properties Research Group, Department of Materials Science and Metallurgy, University of Cambridge, UK for the provision of Neuromat Neural Network software for the present analysis. The insightful suggestions, comments and strong recommendations about the manuscript by the editor and the anonymous reviewers are also gratefully acknowledged. The author received no financial support for the research, authorship, and/or publication of this article. The author declared no potential conflicts of interest with respect to the research, authorship, and/or publication of this article.

References

- T.L. Anderson: Fracture Mechanics: Fundamentals and Applications, CRC Press (2005).
- [2] M.A. Meyers, K.K. Chawla: Mechanical Behaviour of Materials, Cambridge University Press (2009).
- [3] R.T. Qu, Z.J. Zhang, P. Zhang, Z.Q. Liu, Z.F. Zhang: Sci. Rep. 6 (2016). DOI:10.1038/srep23359
- [4] A.A. Griffith: Phil. Trans. R. Soc. Lond. A 221 (1921) 163. DOI:10.1098/rsta.1921.0006
- [5] B. Paul: In Fracture, An Advanced Treatise Vol. II (eds. Liebowitz, H.), Academic Press (1968) 313.
- [6] S.P. Timoshenko: History of Strength of Materials, McGraw-Hill (1953).
- [7] G.R. Irwin, in: Fracturing of Metals by F. Jonassen, W.P. Roop, R.T. Bayless Eds., American Society of Metals (1948) 147.
- [8] R.L. Norton: Design of Machinery: An Introduction to the Synthesis and Analysis of Mechanisms and Machines, McGraw-Hill, Boston (2004). DOI:10.1115/1.1723467
- [9] R.J. Roark, W.C. Young: Formulas for Stress and Strain, McGraw-Hill, Boston (1975).
- [10] R.G. Budynas, J.K. Nisbett: Shigley's Mechanical Engineering Design. McGraw-Hill, New York (2008).
- [11] C. Inglis: SPIE Milest. Ser. MS 137 (1997) 3.
- [12] E. Coker, K. Chakko, Y. Satake: Proc. Inst. Eng. Shipbuild. Scotl. 63 (1919) 34.
- [13] R. Howland: Philos. Trans. R. Soc. Lond. A 229 (1930) 49. DOI:10.1098/rsta.1930.0002
- [14] M. Strandberg: Eng. Fract. Mech. 68 (2001) 577. DOI:10.1016/S0013-7944(00)00101-6
- [15] M. Zappalorto, P. Lazzarin: Eng. Fract. Mech. 78 (2011) 2691. DOI:10.1016/j.engfracmech.2011.07.005
- [16] R. Qu, P. Zhang, Z. Zhang: J. Mater. Sci. Technol. 30 (2014) 599. DOI:10.1016/j.jmst.2014.04.014
- [17] Z.F. Zhang, J. Eckert: Phys. Rev. Lett. 94 (2005) 094301. DOI:10.1103/PhysRevLett.94.094301
- [18] R.T. Qu, Z.F. Zhang: Sci. Rep. 3 (2013). DOI:10.1038/srep01117

- [19] P. Lorenzino, A. Navarro: Int. J. Fatigue 70 (2015) 205. DOI:10.1016/j.ijfatigue.2014.09.012
- [20] T. Nozawa, H. Tanigawa: Int. J. Appl. Ceram. Technol. 7 (2010) 304. DOI:10.1111/j.1744-7402.2009.02469.x
- [21] K. Kumar, A. Pooleery, K. Madhusoodanan, R.N. Singh, A. Chatterjee, B.K. Dutta, R.K. Sinha: Mater. Sci. Eng. A 675 (2016) 32. DOI:10.1016/j.msea.2016.08.032
- [22] P. Lorenzino, A. Navarro: Int. J. Fatigue 71 (2015) 64. DOI:10.1016/j.ijfatigue.2014.03.023
- [23] C.J. Young, D.A. Koss, R.K. Everett: Metall. Mater. Trans. A 33 (2002) 3293. DOI:10.1007/s11661-002-0316-x
- [24] J.Q. Ran, M.W. Fu, W.L. Chan: Int. J. Plast. 41 (2013) 65. DOI:10.1016/j.ijplas.2012.09.002
- [25] J. Lian, H. Yang, N. Vajragupta, S. Münstermann, W. Bleck: Comp. Mater. Sci. 94 (2014) 245. DOI:10.1016/j.commatsci.2014.05.051
- [26] G. Requena, E. Maire, C. Leguen, S. Thuillier: Mater. Sci. Eng. A 589 (2014) 242. DOI:10.1016/j.msea.2013.09.084
- [27] J.W. Hancock, A.C. Mackenzie: J. Mech. Phys. Solids 24 (1976) 147. DOI:10.1016/0022-5096(76)90024-7
- [28] J.R. Rice, D.M. Tracey: J. Mech. Phys. Sol. 17 (1969) 201. DOI:10.1016/0022-5096(69)90033-7
- [29] A. Das, T. Chowdhury, S. Tarafder: Mater. Des. 54 (2014) 1002. DOI:10.1016/j.matdes.2013.09.018
- [30] A. Das, S.K. Das, S. Sivaprasad, M. Tarafder, S. Tarafder: Proc. Eng. 55 (2013) 786. DOI:10.1016/j.proeng.2013.03.332
- [31] G. Sanyal, A. Das, J.B. Singh, J.K. Chakravartty: Mater. Sci. Eng. A 641 (2015) 210. DOI:10.1016/j.msea.2015.06.044
- [32] A. Das: Metall. Mater. Trans. A (2018) 1. DOI:10.1007/s11661-018-4516-4
- [33] A. Das, S. Sivaprasad, M. Ghosh, P.C. Chakraborti, S. Tarafder: Mater. Sci. Eng. A 486 (2008) 283. DOI:10.1016/j.msea.2007.09.005
- [34] A. Das, S. Tarafder: Int. J. Plast. 25 (2009) 2222. DOI:10.1016/j.ijplas.2009.03.003
- [35] A. Das, S. Tarafder: Scr. Mater. 59 (2008) 1014.DOI:10.1016/j.scriptamat.2008.07.012
- [36] A. Das: Scripta Mater. 68 (2013) 514. DOI:10.1016/j.scriptamat.2012.11.039
- [37] A. Das, S. Sivaprasad, P.C. Chakraborti, S. Tarafder: Mater. Sci. Eng. A 528 (2011) 7909. DOI:10.1016/j.msea.2011.07.011
- [38] A. Das, S.K. Das, S. Sivaprasad, S. Tarafder: Scr. Mater. 59 (2008) 681. DOI:10.1016/j.scriptamat.2008.05.043
- [39] A. Das, S. Sivaprasad, P.C. Chakraborti, S. Tarafder: Mater. Sci. Eng. A 496 (2008) 98. DOI:10.1016/j.msea.2008.05.007
- [40] A. Das, S.K. Das, S. Tarafder: Metall. Mater. Trans. A 40 (2009) 3138. DOI:10.1007/s11661-009-9999-6
- [41] A. Das, S. Sivaprasad, P.C. Chakraborti, S. Tarafder: Philos. Mag. Lett. 91 (2011) 664. DOI:10.1080/09500839.2011.608385
- [42] A. Das, N. Roy, A.K. Ray: Mater. Sci. Eng. A 598 (2014) 28.
 DOI:10.1016/j.msea.2013.12.097
- [43] A. Das: Philos. Mag. 97 (2017) 867. DOI:10.1080/14786435.2017.1285072
- [44] A. Das: Philos. Mag. 97 (2017) 3084. DOI:10.1080/14786435.2017.1367857
- [45] A. Das, J.K. Chakravartty: Surf. Topogr. Metrol. Prop. 5 (2017) 045006. DOI:10.1088/2051-672X/aa7931
- [46] A. Das, J.K. Chakravartty: Int. J. Mater. Res. 107 (2016) 184. DOI:10.3139/146.111331
- [47] A. Das: Mater. Sci. Technol. 32 (2016) 1366. DOI:10.1080/02670836.2015.1126048
- [48] A. Das, P. Poddar: Mater. Des. 47 (2013) 557. DOI:10.1016/j.matdes.2012.12.041
- [49] A. Das: Philos. Mag. 95 (2015) 844. DOI:10.1080/14786435.2015.1008069
- [50] A. Das: Metall. Mater. Trans. A 45 (2014) 2927.DOI:10.1007/s11661-014-2295-0
- [51] A. Das: Philos. Mag. 95 (2015) 2210. DOI:10.1080/14786435.2015.1042938
- [52] A. Das: Mater. Sci. Eng. A 658 (2016) 484. DOI:10.1016/j.msea.2016.01.072
- [53] A. Das: Mater. Charact. 123 (2017) 315.DOI:10.1016/j.matchar.2016.11.037

- [54] A. Das: Int. J. Damag. Mech. 27 (2016) 218.DOI:10.1177/1056789516674765
- [55] A. Das: Mater. Res. Exp. 3 (2016) 066501. DOI:10.1088/2053-1591/3/7/079503
- [56] A. Das: J. Mag. Mag. Mater. 361 (2014) 232. DOI:10.1016/j.jmmm.2014.02.006
- [57] A. Das: Int. J. Fatigue 70 (2015) 473. DOI:10.1016/j.ijfatigue.2014.06.012
- [58] A. Das: PhD Thesis, Phase transformation during tensile and low cycle fatigue deformation of AISI 304LN stainless steel, Jadavpur University, Kolkata (2013).
- [59] C. Betegon, J.W. Hancock: J. Appl. Mech. 58 (1991) 104. DOI:10.1115/1.2897135
- [60] N.P. O'Dowd, C.F. Shih: Two-parameter fracture mechanics: theory and applications. In Fracture Mechanics, Vol. 24, ASTM International (1994). DOI:10.1520/STP13698S
- [61] W.D. Pilkey: Peterson's stress concentration factors (2003).
- [62] W.C. Young, R.G. Budynas: Roark's formulas for stress and strain, Vol. 7, New York: McGraw-Hill (2002).
- [63] F.K. Chang, K.Y. Chang: J. Compos. Mater. 21 (1987) 834. DOI:10.1177/002199838702100904
- [64] M.J. Blackburn: Relationship of microstructure to some mechanical properties of Ti-8Al-1V-1Mo, Boeing Scientific Research Labs., Seattle (1966).
- [65] G.R. Yoder, L.A. Cooley, T.W. Crooker: Eng. Fract. Mech. 11 (1979) 805. DOI:10.1016/0013-7944(79)90138-3
- [66] Z. Foroulis: Environment-sensitive fracture of engineering materials, In Fall Meeting of the Metallurgical Society of AIME (1977).
- [67] W.D. Jenkins, W.A. Willard: NBS J Engg. Instrum. 73 (1966) 5.
- [68] T.R. Wilshaw, P.L. Pratt: J. Mech. Phys. Sol. 14 (1966) 7. DOI:10.1016/0022-5096(66)90015-9
- [69] T.R. Wilshaw, C.A. Rau, A.S. Tetelman: Engg. Fract. Mech. 1 (1968) 191. DOI:10.1016/0013-7944(68)90025-8
- [70] R. Hill: The mathematical theory of plasticity, Vol. 11, Oxford University Press (1998).
- [71] D.J.C. MacKay: Neural. Comput. 4 (1992) 415. DOI:10.1162/neco.1992.4.3.415
- [72] D.J.C. MacKay: Neural. Comput. 4 (1992) 448. DOI:10.1162/neco.1992.4.3.448
- [73] D.J.C. MacKay: ASHRAE Trans. 100 (1994) 1053. DOI:10.1.1.47.5125
- [74] D.J.C. MacKay: Network: Comp. Neu. Sys. 6 (1995) 469. DOI:10.1088/0954-898X_6_3_011
- [75] H. Fujii, D.J.C. Mackay, H.K.D.H. Bhadeshia: ISIJ Int. 36
- (1996) 1373. DOI:10.2355/isijinternational.36.1373
 [76] R.C. Eberhart, R.W. Dobbins: Implementations. In Neural network PC tools, Academic Press Professional, Inc (1990) 35.
- DOI:10.1016/B978-0-12-228640-7.50008-8
 [77] A.Y. Badmos, H.K.D.H. Bhadeshia, D.J.C. MacKay: Mater. Sci. Technol. 14 (1998) 793. DOI:10.1179/mst.1998.14.8.793
- [78] H.K.D.H. Bhadeshia: ISIJ Int. 39 (1999) 966. DOI:10.2355/isijinternational.39.966
- [79] H.K.D.H. Bhadeshia, R.C. Dimitriu, S. Forsik, J.H. Pak, J.H. Ryu: Mater. Sci. Technol. 25 (2009) 504. DOI:10.1179/174328408X311053
- [80] A. Das, S. Tarafder, P.C. Chakraborti: Mater. Sci. Eng. A 529 (2011) 9. DOI:10.1016/j.msea.2011.08.039
- [81] A. Das, P.C. Chakraborti, S. Tarafder, H.K.D.H. Bhadeshia: Mater. Sci. Technol. 27 (2011) 366. DOI:10.1179/026708310X12668415534008
- [82] A. Das, S. Sivaprasad, M. Tarafder, S.K. Das, S. Tarafder: Appl. Soft Comput. 13 (2013) 1033. DOI:10.1016/j.asoc.2012.09.016
- [83] A. Das: Metall. Mater. Trans. A 47 (2016) 748. DOI:10.1007/s11661-015-3266-9
- [84] A. Das: J. Mater. Eng. Perform. 26 (2017) 2708. DOI:10.1007/s11665-017-2695-6
- [85] A. Das: Mater. Sci. Tech. (2018). DOI:10.1080/02670836.2017.1418476
- [86] B.P. Arjyal, D.G. Katerelos, C. Filiou, C. Galiotis: Exp. Mech. 40 (2013) 248. DOI:10.1007/BF02327496
- [87] G.K. Haritos, T. Nicholas, D.B. Lanning: Int. J. Fatigue 21 (1999) 643. DOI:10.1016/S0142-1123(99)00023-7

- [88] G.Z. Wang, Y.L. Wang: Int. J. Fract. 146 (2008) 105. DOI:10.1007/s10704-007-9151-9
- [89] A.S. Tetelman, T.R. Wilshaw, C.A. Rau: Jr. Int. J. Fract. Mech. 4 (1968) 147. DOI:10.1007/BF00188941
- [90] J.J. Lewandowski, A.W. Thompson: Metall. Mater. Trans. A 17 (1986) 1769. DOI:10.1007/BF02817275
- [91] P. Bridgman: Trans. ASM. 32 (1944) 553.
- [92] M. Creager: PhD Thesis, The elastic stress field near the tip of a blunt crack, Lehigh University, Pennsylvania, USA (1966).
- [93] F. Bohner, J.K. Gregory, U. Weber, S. Schmauder: Mech. Mater. 31 (1999) 627. DOI:10.1016/S0167-6636(99)00026-5
- [94] A. Kochendorfer, A. Schurenkamper: Arch. Eisenhuttenwesen 32 (1961) 681. DOI:10.1002/srin.196103261
- [95] H. Dietmann: Venia Legendi Dissertation, Calculation of flow curves of components for small deformations, University of Stuttgart, Keplerstraße, Germany (1968).
- [96] W. Backasch, E. Macherauch: Arch. Eisenhuttenwesen 50 (1979) 167. DOI:10.1002/srin.197904720
- [97] J.D. Lubahn: Trans. ASME (1957) 111. DOI:10.1115/1.3605059
- [98] P. Hähner, A. Ziegenbein, E. Rizzi, H. Neuhäuser: Phys. Rev. B 65 (2002) 134109. DOI:10.1103/PhysRevB.65.134109
- [99] L.A. Carlsson, C.G. Aronsson, J. Bäcklund: J. Mater. Sci. 24 (1989) 1670. DOI:10.1007/BF01105690
- [100] J.M. Whitney, R.J. Nuismer: J. Compos. Mater. 8 (1974) 253. DOI:10.1177/002199837400800303
- [101] M. Oyane, S. Shima, Y. Kono: Bulletin of JSME. 16 (1973), 1254. DOI:10.1299/jsme1958.16.1254
- [102] S. Timoshenko: Strength of Materials, Parts I & II (1955).
- [103] T. Majima, M. Anzai, H. Nakazawa: Bulletin of JSME 29 (1986) 4000. DOI:10.1299/jsme1958.29.4000
- [104] A. Needleman: Mech. Mater. 116 (2018) 180. DOI:10.1016/j.mechmat.2016.09.007
- [105] S. Graff, S. Forest, J.L. Strudel, C. Prioul, P. Pilvin, J.L. Béchade: Scr. Mater. 52 (2005) 1181. DOI:10.1016/j.scriptamat.2005.02.007
- [106] S. Graff, S. Forest, J.L. Strudel, C. Prioul, P. Pilvin, J.L. Béchade: Mater. Sci. Eng. A 387 (2004) 181. DOI:10.1016/j.msea.2004.02.083

- [107] J.G. Milke, J.L. Beuth, N.E. Biery: Exp. Mech. 40 (2000) 415. DOI:10.1007/s11661-999-0148-z
- [108] D.A. Knaul, J.L. Beuth, J.G. Milke: Metall. Mater. Trans. A 30 (1999) 949. DOI:10.1007/s11661-999-0148-z
- [109] T.L. Anderson: Int. J. Fract. 41 (1989) 79. DOI:10.1007/BF00018479
- [110] F. Sui, R. Sandström: Mater. Sci. Eng. A 663 (2016) 108. DOI:10.1016/j.msea.2016.03.111
- [111] P. Maj, J. Zdunek, J. Mizera, K.J. Kurzydlowski: Mater. Charact. 96 (2014) 46. DOI:10.1016/j.matchar.2014.07.007

(Received October 25, 2017; accepted April 30, 2018; online since October 2, 2018)

Correspondence address

Dr. Arpan Das, Scientific Officer E
Mechanical Metallurgy Division, Materials Group
Bhabha Atomic Research Centre (Department of Atomic Energy)
Trombay, Mumbai 400 085, Maharashtra
India

Tel.: +91-(0)2225592907/2170 Fax: +91-(0)2225505151 E-Mail: dasarpan1@yahoo.co.in arpand@barc.gov.in

Bibliography

DOI 10.3139/146.111694 Int. J. Mater. Res. (formerly Z. Metallkd.) 109 (2018) 11; page 979–1004 © Carl Hanser Verlag GmbH & Co. KG ISSN 1862-5282